2019

A DUAL STATE HIERARCHICAL ENSEMBLE KALMAN FILTER ALGORITHM

William J. Cook
University of Montana, Missoula

Jesse Johnson
University of Montana, Missoula

Marko Maneta
University of Montana, Missoula

Doug Brinkerhoff
University of Montana, Missoula

A DUAL STATE HIERARCHICAL ENSEMBLE KALMAN FILTER ALGORITHM

By

WILLIAM JOHN COOK

Bachelor of Music, University of Montana, Missoula, Montana, 2017

Thesis

presented in partial fulfillment of the requirements

for the degree of

Master of Science

in Computer Science

The University of Montana

Missoula, MT

December 2019

Approved by:

Scott Whittenburg, Dean of The Graduate School

Graduate School

Jesse Johnson, Chair

Computer Science

Marco Maneta

Geosciences

Douglas Brinkerhoff

Computer Science

0.1 Abstract

Cook, William, M.A, Fall 2019 Computer Science

A Dual State Hierarchical Ensemble Kalman Filter Algorithm

Chairperson: Jesse Johnson

Dynamic models that simulate processes across large geographic locations, such as hydrologic models, are often informed by empirical parameters that are distributed across a geographical area and segmented by geological features such as watersheds. These parameters may be referred to as spatially distributed parameters. Spatially distributed parameters are frequently spatially correlated and any techniques utilized in their calibration ideally incorporate existing spatial hierarchical relationships into their structure. In this paper, a parameter estimation method based on the Dual State Ensemble Kalman Filter called the Dual State Hierarchical Ensemble Kalman Filter (DSHEnKF) is presented. This modified filter is innovative in that it allows parameters to be placed into a set of groups that are smoothed using hierarchical modeling techniques. The usability and effectiveness of this new technique is demonstrated by applying it to a rainfall-runoff model that simulates subcatchment-scale hydrologic processes and contains high dimensional spatially distributed empirical parameters.

Contents

Symbols

$\mathbf{x}^-$	vector of states, pre-correction
$\mathbf{x}^+$	vector of states, post-correction
$\mathbf{y}$	vector of predicted states
θ^-	vector of parameters, pre-correction
θ^+	vector of parameters, post-correction
Υ	A vector of size θ sampled from the grand mean and grand standard deviation of all members of θ across all ensembles of θ
$\mathbf{u}$	vector of forcing data
$\mathbf{z}$	vector of observed states
i	ensemble member
t	timestep
ε	vector of error: model uncertainty
δ	vector of error: observed uncertainty
Q	forcing data error covariance matrix
R	observation error covariance matrix
a	Kernel smoothing mixing parameter
α	Hierarchical parameter perturbation mixing parameter vector
b	Hierarchical parameter perturbation mixing parameter
g	Hierarchical group

G_g	Set of vectors in hierarchical group g
$f()$	Model function
$h()$	Masking function (allows comparison of observations and matching states)
K	Kalman gain matrix
Σ	Shorthand for covariance

Chapter 1

Introduction

Utilizing sequential data assimilation techniques to filter the output of hydrologic models is an efficient way to correct and calibrate hydrologic models before and after their implementation in scientific studies or public projects [30], [26], [29]. Observations such as SWE (snow water equivalent), streamflow, and precipitation are collected on a daily basis across various geographic regions, allowing real time information to be dynamically ingested by the hydrologic model and inform present and future predictions. Hydrologic models allow hydrologists to better understand the catchment hierarchy and predict the response, and the need to research optimal methods of hydrologic data assimilation has been recognized [37] and researched [20], [29]. Observed hydrologic data may allow models that output streamflow or SWE states, such as rainfall-runoff models, to undergo parameter estimation. Many empirical parameters exist in conceptual hydrologic models, such as the HBV model, to account for wildcard environmental attributes such as the temperature threshold for melting snow in a snowpack system [21], the percolation of water from the upper to the lower reservoir of a groundwater system [21], or the dispersion of a wave through a channel used in the Muskingham-Cunge routing method [25]. These parameters are frequently correlated and can have more then one set of values that produce good results [15], [21]. Parameter estimation for rainfall-runoff models has been an active area of research [34],[35] and research has progressed into the 21st century [26], [39], [29].

Models that ingest data sequentially can have their variables efficiently refined, a process henceforth referred to as 'filtering', by a Kalman Filter, a sequential data assimilation algorithm. Kalman Filters only need the previous timestep's state estimate and covariance matrices to update the current timestep's state estimate and covariance matrices based on a new observed state. The original Kalman filter[18] was created for applications on linear systems and adaptations are necessary for applications to non-linear systems. The extended Kalman Filter[16] works for mildly non-linear systems but does not function optimally on strongly non-linear systems[24]. The Unscented Kalman Filter[17] is an improvement on the Extended Kalman Filter that allows for the filtering of highly non-linear systems by using weighted samples from the state distribution. The Ensemble Kalman Filter[10], a predecessor to the Unscented Kalman Filter, filters non-linear systems by generating an 'ensemble' of model instances and adding unique noise to each instance's forcing data. An advantage of this ensemble based approach is the EnKF's capacity to approximate the complete posterior estimation of a problem without weighting the samples, resulting in a better handling of strong non-linearity. The substitution of the original Kalman Filter's error covarience matrix with an ensemble covariance matrix also allows for the efficient computation of the covariance of high dimensional state vectors.

To calibrate model parameters as well as correct model states a Dual State Kalman Filter may be used as demonstrated by Moradkhani et. al in 2005 [26]. Dual state Kalman filters simulate parameter perturbation by adding a small unbiased and Gaussian perturbation to the model parameters . These perturbed parameters vectors are then corrected in a similar fashion to the state vectors. After this happens a second filter is run to correct the state vectors in the traditional fashion. The Dual State Ensemble Kalman Filter implemented by Moradkhani et. al[26] extends the Ensemble Kalman Filter into a dual state configuration and is shown to successfully predict a set of parameters and correct model predictions.

An alternative method of dual parameter and state estimation that utilizes the Kalman Filter is the Joint Kalman Filter, which combines states and parameters into one vector that is calculated simultaneously without the need for a second run. Joint

Ensemble Kalman Filters have been successfully implemented on hydrologic models [38], [43] and other models [8], but Joint Ensemble Kalman filters can suffer from "filter inbreeding" under certain circumstances [14] [41]. Overall Dual Ensemble Kalman Filters have been shown to produce more accurate parameter estimations then Joint Ensemble Kalman Filters, especially in noisy situations or non-linear environments, with the major drawback of the Dual approach being its larger computational cost [22].

1.1 Aim

When semidistributed hydrologic models are applied over large regions that are sparsely gauged, calibrated model parameters need to be transferred from subcatchments where parameters have been identified - such as in gauged subcatchments where observations exist - to neighboring ungaged subcatchments where observations are not known in a process generally referred to as regionalization [7], [23]. Generally, regionalization techniques transfer information between catchments deemed to be similar in some way. Multiple methods of classifying catchments as similar include by using spatial proximity [17] or through other catchment attributes such as catchment shape or topographic characteristics [28]. However, the correlation of catchment attributes with catchment parameters are typically low [3] and can result in low model performances [32], [4]. The regionalization problem in hydrologic modeling is not solved yet and is currently an important area of research in hydrology [3], [13].

In this paper, hierarchical modeling techniques are integrated into the Dual State Ensemble Kalman Filter's parameter perturbation equation to create a Hierarchical Dual State Ensemble Kalman Filter. A hierarchical parameter perturbation framework allows the model to account for parameters that are potentially hierarchically related. For example, streamflow wave celerity being calculated for a series of subbasins may be hierarchically related to each other because of a larger watershed or topographic feature enveloping them. To examine the Dual State Hierarchical Ensemble Kalman Filter's application to high dimensional spatially distributed raster

data and geographical data the hydrologic model, a variation of a rainfall-runoff model, is implemented to predict streamflows across the state of Montana. The hydrologic model is informed by a variety of sub-components featuring high dimensional spatially distributed parameters, including a snowpack process, soil process, and a Muskingham-Cunge routing component. The hydrologic model's parameters can be linked to individual sub-basins with can in turn be sorted into hydrologic unit code watershed boundaries.

Chapter 2 covers the methods behind the Dual State Hierarchical Ensemble Kalman Filtering algorithm. Chapter 3 discusses the hydrologic model and how a Dual State Hierarchical Ensemble Kalman Filter was applied to it. Chapter 4 presents results while Chapter 5 discusses conclusions and further research opportunities.

Chapter 2

The Hierarchical Dual Ensemble Kalman Filter Method

2.1 General Dynamic Model and Observations

A generic dynamic model can be defined as one more more discrete nonlinear stochastic processes[8]:

$$\boldsymbol{x_{t+1}} = f(\boldsymbol{x_t}, \boldsymbol{u_t}, \boldsymbol{\theta_t}) + \varepsilon_{\boldsymbol{t}} \tag{2.1}$$

where $\boldsymbol{x_t}$ is an n dimensional vector representing the state variables of the model at time step $\boldsymbol{t}$, $\boldsymbol{u_t}$ is a vector of forcing data (e.g temperature or precipitation) at time step $\boldsymbol{t}$, and $\boldsymbol{\theta_t}$ is a vector of model parameters which may or may not change per time step (e.g soil beta - β or degree day factor - DDF). The non-linear function f takes these variables as inputs and returns the updated state vector at the next timestep $\boldsymbol{x_{t+1}}$. The noise variable $\varepsilon_{\boldsymbol{t}}$ accounts for both model structural error and for any uncertainty in the forcing data.

A state's observation vector $\boldsymbol{z_t}$ can be defined as

$$\boldsymbol{z_t} = h(\boldsymbol{x_t}, \boldsymbol{\theta_t}) + \delta_{\boldsymbol{t}} \tag{2.2}$$

Where the $\boldsymbol{x_t}$ vector represents the true state, $\boldsymbol{\theta_t}$ represents the true parameters,

$h(.)$ is a function that determines the relationship between observation and state vectors, and $\delta_{\boldsymbol{t}}$ represents observation error. $\delta_{\boldsymbol{t}}$ is Gaussian and independent of $\varepsilon_{\boldsymbol{t}}$.

The Dual Hierarchical State Ensemble Kalman Filter can be split into three subsections: The prediction phase, the parameter correction phase, and the state correction phase.

2.2 DEnHKF Method

2.2.1 Prediction Phase

Just as in a standard Dual Ensemble Kalman filter [26], each ensemble member $\boldsymbol{i}$ is represented by a stochastic model similar to (2.1). The modified equation is as follows:

$$\boldsymbol{x}_{\boldsymbol{t+1}}^{\boldsymbol{i-}} = f(\boldsymbol{x}_{\boldsymbol{t}}^{\boldsymbol{i+}}, \boldsymbol{u}_{\boldsymbol{t}}^{\boldsymbol{i}}, \boldsymbol{\theta}_{\boldsymbol{t}}^{\boldsymbol{i-}}) + \omega_{\boldsymbol{t}}, \quad \boldsymbol{i} = 1, ..., n \tag{2.3}$$

Where n is the total number of ensembles. The $-/+$ superscripts denote filtered $(+)$ and uncorrected $(-)$ values. Note that $\boldsymbol{\theta}_{\boldsymbol{t}}^{\boldsymbol{i-}}$'s $\boldsymbol{t}$ subscript does not necessarily denote that θ is time dependent when implemented in the standalone model but rather indicates that parameter values change as they are filtered over time. The noise term ω_t accounts for model error. Since the model error is unknown, ω_t is hereafter excluded from the prediction equation. Model error is accounted for via the perturbation of the forcing data, see below [11].

Errors in the model design and process noise are accounted for through the perturbation the forcing data vector $\boldsymbol{u}_{\boldsymbol{t}}$ with random noise $\zeta_{\boldsymbol{t}}^{\boldsymbol{i}}$ to generate a unique vector $\boldsymbol{u}_{\boldsymbol{t}}^{\boldsymbol{i}}$ for each ensemble [26], [8]. ζ_t^i is drawn from a normal distribution with a covarience matrix $Q_{\boldsymbol{t}}^{\boldsymbol{i}}$.

$$\boldsymbol{u}_{\boldsymbol{t+1}}^{\boldsymbol{i}} = \boldsymbol{u}_{\boldsymbol{t}} + \zeta_t^i, \quad \zeta_t^i \sim N(0, Q_t^i) \tag{2.4}$$

Parameter Perturbation

To generate the apriori parameters $\boldsymbol{\theta}_{\boldsymbol{t+1}}^{\boldsymbol{i-}}$, an evolution of the parameters similar to the evolution of the state variables must be implemented. Implementations of parameter evolution in [36] added a small perturbation sampled from $N(0, \Sigma_t^\theta)$, where Σ_t^θ represents the covariance matrix of θ at timestep t. This legacy method of evolution resulted in overly dispersed parameter samples and the loss of continuity between two consecutive points in time [19] [8]. To overcome this the kernel smoothing technique developed by West [42] and implemented by Liu [19] has been used effectively in previous Dual Ensemble Kalman filter implementations [26] and similar models [8].

$$\boldsymbol{\theta}_{\boldsymbol{t+1}}^{\boldsymbol{i-}} = a\boldsymbol{\theta}_{\boldsymbol{t}}^{\boldsymbol{i+}} + (1-a)\bar{\boldsymbol{\theta}}_{\boldsymbol{t}}^{+} + \boldsymbol{\tau}_{\boldsymbol{t}}^{\boldsymbol{i}} \tag{2.5}$$

$$\boldsymbol{\tau}_{\boldsymbol{t}}^{\boldsymbol{i}} \sim N(0, h^2 V_t) \tag{2.6}$$

Where $\bar{\boldsymbol{\theta}}_{\boldsymbol{t}}^{+}$ is the mean of the parameters with respect to the ensembles, $V_t = \text{var}(\boldsymbol{\theta}_{\boldsymbol{t}}^{\boldsymbol{i}+})$, a is a shrinkage factor between (0,1) of the kernel location, and h is a smoothing factor. h may be defined as $\sqrt{1-a^2}$. In previous research a values chosen between .45 and .49 have been shown to be optimal [8], but note that h and a tend to vary per model and are generally found via experimentation [26] [1] [2] [8].

Hierarchical Parameter Perturbation

In a standard hierarchical linear regression, a value y and its predictor variables α and β are contained in vectors $\boldsymbol{g_y}$, $\boldsymbol{g_\alpha}$, and $\boldsymbol{g_\beta}$ respectively, all of which are of size $N, j = 1, ..., n$. Vectors g_α and g_β have a mean and standard deviation of $\mu_\alpha, \sigma_\alpha$ and μ_β, σ_β respectively.

$$y_{j,g} = \alpha_g x_{j,g} + \beta_g, \quad \alpha_g \in N(\mu_\alpha, \sigma_\alpha), \quad \beta_g \in N(\mu_\beta, \sigma_\beta) \tag{2.7}$$

where α and β are determined to be hierarchically related properties drawn from their respective normal distributions. For a simple overview of hierarchical models refer to Osborne [27], while [12] is a more in-depth reference.

In a Hierarchical Duel Ensemble Kalman Filter, parameter perturbation has been modified to have properties of a hierarchical linear regressive system. First, all individual components of the vector θ are sorted into m new vectors defined by hierarchical belonging, where m is the total number of hierarchical groups. All new vectors are part of set G. A subset of G where all selected members are in the same hierarchical group is henceforth referred to as G_g. Each member j of a group vector G_g, where g is the specific group number, is related to other members through shared hierarchical characteristics (spatial or otherwise.) Algorithms (2.5) and (2.6) are then updated to conform to the hierarchical structure described in (2.7):

$$\boldsymbol{\theta}^{\boldsymbol{i-}}_{\boldsymbol{t+1,g}} = a\boldsymbol{\Upsilon}^{\boldsymbol{i}}_{\boldsymbol{t,g}} + (1-a)\bar{\boldsymbol{\theta}}^{\boldsymbol{+}}_{\boldsymbol{t,g}} + \boldsymbol{\tau}^{\boldsymbol{i}}_{\boldsymbol{t,g}} \tag{2.8}$$

$$\boldsymbol{\Upsilon}^{\boldsymbol{i}}_{\boldsymbol{t,g}} \sim N(\mu_g, \sigma_g) \tag{2.9}$$

$$\boldsymbol{\tau}^{\boldsymbol{i}}_{\boldsymbol{t}} \sim N(0, h^2 V^i_{t,g}) \tag{2.10}$$

Where $\bar{\boldsymbol{\theta}}^{\boldsymbol{i+}}_{\boldsymbol{t,g}}$ is the mean over all ensembles for all members of group g, μ_g and σ_g are the grand mean and grand standard deviation respectively of all ensembles and locations in the set of vectors in G_g (for clarity, the calculation of the grand mean and grand standard deviation returns a scalar value), and $V_{g,t}$ is the variance matrix with respect to the ensembles of all members of group g.

The final modification to be made allows for the dynamic calculation of the shrinkage factor a. Since $\boldsymbol{\tau}^{\boldsymbol{i}}_{\boldsymbol{t}}$ is dependent on the standard deviation of the ensemble $\boldsymbol{\theta}^{\boldsymbol{i+}}_{\boldsymbol{t,g}}$, a group of ensembles that have tightened around a group of parameters will be increasingly be drawn to the grand mean μ_θ, decoupling tight ensembles from their chosen values and ultimately causing all values across a hierarchical group to collapse to one value. To prevent this, a vector α is substituted for a such that

$$\boldsymbol{\alpha}^{\boldsymbol{i}}_{\boldsymbol{t,g}} = a[\frac{2}{1+e^{-b\boldsymbol{v}}} - 1] \tag{2.11}$$

where $\boldsymbol{v}$ is a vector of variances with respect to the ensembles of all members in group g and b is a tuning parameter that controls how quickly $e^{-b\boldsymbol{v}}$ converges to 0. b must be chosen very carefully and will vary from parameter to parameter, with the simple equation $b = 1/totalrange$ acting as a possible starting point. All members of vector $\boldsymbol{\alpha}^{\boldsymbol{i}}_{\boldsymbol{t,g}}$ will fall between 0 and a, with a being a value < 1.

Thus, the final equation is

$$\boldsymbol{\theta}^{\boldsymbol{i-}}_{\boldsymbol{t+1,g}} = \boldsymbol{\alpha}\boldsymbol{\Upsilon}^{\boldsymbol{i}}_{\boldsymbol{t,g}} + (1 - \boldsymbol{\alpha})\bar{\boldsymbol{\theta}}^{\boldsymbol{+}}_{\boldsymbol{t,g}} + \boldsymbol{\tau}^{\boldsymbol{i}}_{\boldsymbol{t,g}} \tag{2.12}$$

2.2.2 Parameter Correction Phase

In an Ensemble Kalman Filter, observations are perturbed to reflect model error. To accomplish this n unique perturbations are created. Therefore, the variable $\boldsymbol{z}^{\boldsymbol{i}}_{\boldsymbol{t+1}}$ is defined as follows:

$$\boldsymbol{z}^{\boldsymbol{i}}_{\boldsymbol{t+1}} = \boldsymbol{z}_{\boldsymbol{t+1}} + \boldsymbol{\eta}^{\boldsymbol{i}}_{\boldsymbol{t+1}}, \quad \boldsymbol{\eta}^{\boldsymbol{i}}_{\boldsymbol{t+1}} = N(0, R_{t+1}) \tag{2.13}$$

Where z_{t+1} is an observation vector defined by (2.2) and η^i_{t+1} is a random perturbation drawn from a normal distribution with covarience matrix R_{t+1}. A set of state predictions that can be related to the observations are generated by running the a priori state vector through the function $h(.)$:

$$\hat{\boldsymbol{y}}^{\boldsymbol{i}}_{\boldsymbol{t+1}} = h(\boldsymbol{x}^{\boldsymbol{i-}}_{\boldsymbol{t+1}}, \boldsymbol{\theta}^{\boldsymbol{i-}}_{\boldsymbol{t+1}}) \tag{2.14}$$

The parameter update equation is similar to the update equation of the linear Kalman filter $\boldsymbol{x}^{+}_{\boldsymbol{t}} = \boldsymbol{x}^{-}_{\boldsymbol{t}} + K_t(\boldsymbol{z_t} - H\hat{\boldsymbol{x}}_{\boldsymbol{t}})$, with $\hat{\boldsymbol{y}}^{\boldsymbol{i}}_{\boldsymbol{t+1}}$ serving the same purpose as $H\hat{\boldsymbol{x}}_{\boldsymbol{t}}$. However, unlike the linear kalman filter, parameters are corrected in lieu of the states in the first correction phase:

$$\boldsymbol{\theta}^{\boldsymbol{i+}}_{\boldsymbol{t+1}} = \boldsymbol{\theta}^{\boldsymbol{i-}}_{\boldsymbol{t+1}} + K^{\theta}_{t+1}(\boldsymbol{z}^{\boldsymbol{i}}_{\boldsymbol{t+1}} - \hat{\boldsymbol{y}}^{\boldsymbol{i}}_{\boldsymbol{t+1}}) \tag{2.15}$$

To facilitate this, K^{θ}_{t+1} is defined as

$$K_{t+1}^{\theta} = \Sigma_{t+1}^{\theta,\hat{y}}(\Sigma_{t+1}^{\hat{y},\hat{y}} + R_{t+1})^{-1} \tag{2.16}$$

where $\Sigma_{t+1}^{\theta,\hat{y}}$ is the cross covariance of $\boldsymbol{\theta_{t+1}}$ and $\boldsymbol{\hat{y}_{t+1}}$, $\Sigma_{t+1}^{\hat{y},\hat{y}}$ is the covarience of $\boldsymbol{\hat{y}_{t+1}}$, and R_{t+1} is the observation error matrix from (2.13).

2.2.3 State Correction Phase

After $\boldsymbol{\theta_{t+1}^{i+}}$ has been calculated the model is run again (2.3) with the $\boldsymbol{\theta_{t+1}^{i+}}$ replacing $\boldsymbol{\theta_{t+1}^{i-}}$.

$$\boldsymbol{x_{t+1}^{i-}} = f(\boldsymbol{x_t^{i+}}, \boldsymbol{u_t^i}, \boldsymbol{\theta_t^{i+}}), \quad i = 1, ..., n \tag{2.17}$$

After a new state vector is generated it is re-run through (2.14) with the new parameter vector:

$$\boldsymbol{\hat{y}_{t+1}^i} = h(\boldsymbol{x_{t+1}^{i-}}, \boldsymbol{\theta_{t+1}^{i+}}) \tag{2.18}$$

The corrected state vector is then run through the state update equation

$$\boldsymbol{x_{t+1}^{i+}} = \boldsymbol{x_{t+1}^{i-}} + K_{t+1}^{x}(\boldsymbol{z_{t+1}^i} - \boldsymbol{\hat{y}_{t+1}^i}) \tag{2.19}$$

$$K_{t+1}^{x} = \Sigma_{t+1}^{x,\hat{y}}(\Sigma_{t+1}^{\hat{y},\hat{y}} + R_{t+1})^{-1} \tag{2.20}$$

where $\Sigma_{t+1}^{x,\hat{y}}$ is the cross covariance of $\boldsymbol{x_{t+1}}$ and $\boldsymbol{\hat{y}_{t+1}}$.

Chapter 3

Application of DHEnKF to Hydrologic Model

3.1 The Hydrologic Model

The hydrologic model is used to test the viability of the DSHEnKF method. The hydrologic model takes parameters related to streamflows and groundwater, precipitation, minimum daily temperatures, and maximum daily temperatures as inputs and outputs streamflow values along with some additional states such as the amount of water precipitated as snowfall (henceforth referred to as `swe` or snow water equivalent.) The hydrologic model was designed to be implemented in any geographic location. For this study it was utilized to model streamflows throughout the western half of the state of Montana.

Configuring the hydrologic model to model streamflows throughout Western Montana is advantageous because it allows for the calibration of a very large number of spatially distributed, high dimensional parameters. These parameters can be ex-

Table 3.1: States

State	Dimensions
Streamflow (in cubic meters per second)	66 (nodes)
Snow Water Equivalent (in mm^3)	12319 (pixels)

Table 3.2: Forcing Data

Forcing Data (u)	Purpose	Dimensions
tempmin	Lowest temperature for timestep	12319 (pixels)
tempmax	Highest temperature for timestep	12319 (pixels)
precipitation	Amount of rainfall for timestep	12319 (pixels)

pected to vary significantly across the entirety of Western Montana, a mountainous region which covers an area of over 80,000 km^2 and sports diverse terrain.

3.1.1 Input Data

The hydrologic model takes rasterized precipitation data and temperature data from meteorological databases as input. This data (Table 3.2) was utilized as a vector of forcing data in the ensemble kalman filter framework (e.g: $u_t = [precip_t, Tmin_t, Tmax_t]$.)

3.1.2 Calibrated Parameters

The hydrologic model utilizes a HBV rainfall-runoff component and a Muskingum-Cunge routing component. The HBV component includes a precipitation and snow-pack process that utilizes the empirical parameters degree day factor (mm°C^{-1}d^{-1}) and temperature threshold (°C), a soil process that utilizes the empirical parameters potential evapo-transpiration (dimensionless), soil beta (dimensionless), and soil max water content (mm), and a runoff generation process that utilizes the empirical parameters $ck0$ (d^{-1}), $ck1$ (d^{-1}), $ck2$ (d^{-1}), $hl1$ (mm), and $perc$ (d), all of which control various aspects of groundwater percolation and runoff. The Muskingum-Cunge routing component utilizes parameters that control wave dispersion (dimensionless) and wave celerity (seconds). Wave celerity was not calibrated in this project. To learn more about the hydrologic model, its algorithms, and the parameters that control it refer to Appendix A.

Table 3.3: Calibrated Parameters

Parameter (θ)	Purpose
`ddf`	Degree Day Factor
`aet_lp`	Potential Evapo-Transpiration
`soil_beta`	Portion of ponded water that goes into soil storage
`soil_max_wat`	Soil compartment maximum water capacity
`ck0`	Immediate runoff
`ck1`	Fast runoff
`ck2`	Groundwater runoff
`hl1`	Groundwater water storage threshold
`perc`	Groundwater peculation
`e`	Wave dispersion

Table 3.4: Observations

Observed State (x)	Source	Dimensions
streamflow	USGS	26
snow water equivalent	NRCS	45

3.2 Observation Data

A Kalman Filter relies on one or more observed states for correction. Accordingly, observations were obtained for streamflows and snowfall across Montana. For streamflow, USGS streamflow data was collected at 26 sites. Each observed site was paired with the closest simulated stream outlet within a 2.5 mile cutoff. For snowfall, SNOTEL sites monitored by the Natural Resources Conservation Service (NRCS) were used 3-1. 45 stations were chosen and matched to specific pixels in the hydrologic model's raster files.

3.3 Catchment Data and Hierarchical Groups

The hydrologic model utilizes the Watershed Boundary Dataset (WBD), a national hydrologic unit from the USGS that defines the areas of the United States landscape that drain to portions of the stream network, to separate Montana into 330 watersheds, each with its own stream reach (Figure 3-2.) Each watershed is associated with one of each type of parameter from Table 3.3. These 330 watersheds fall into

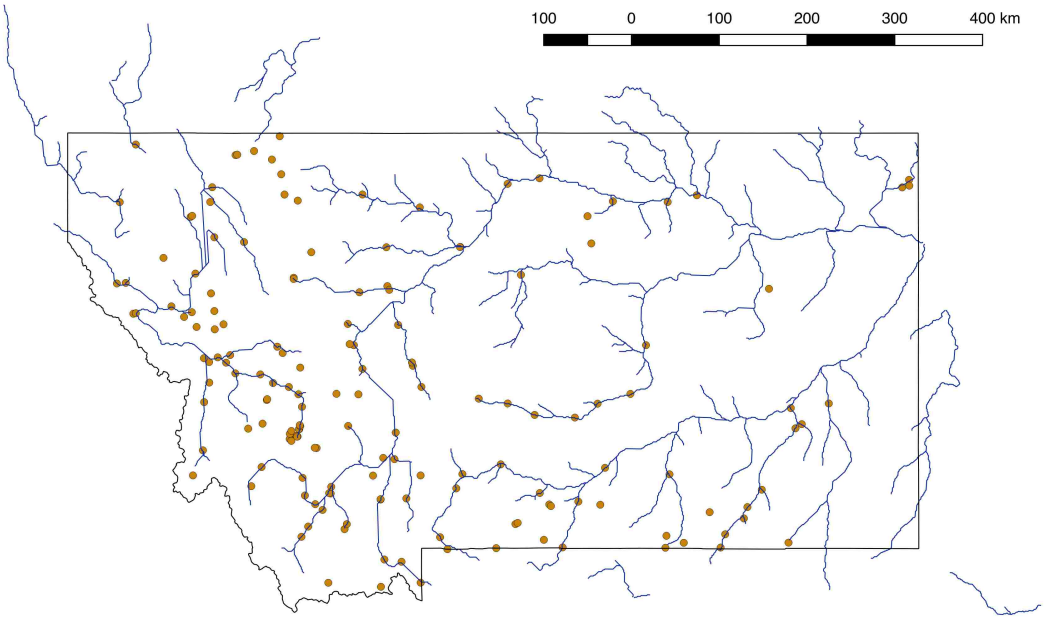

Figure 3-1: `swe` stations (orange dots) and modeled streamflows across all of Montana. The streamflows and `swe` stations in the western section of Montana (shown in blue in figure 3-3) were utilized for this project.

3 larger watershed zones (called HUC4, or 4-digit hydrologic unit boundaries) that were utilized to classify each watershed into one of 3 hierarchical zones (Figure 3-3.) For this project the leftmost HUC-4 zone (shown in blue in figure 3-3) was utilized to obtain the 66 hydrologic HUC-8 watersheds used in the hydrologic model.

3.4 Small Testset

A filtering run could take anywhere between 20 hours and a week depending on calibration duration and number of ensembles used. In order to efficiently test new equations and starting parameters a small 3 node dataset was developed. This dataset covered the Bitterroot area of Montana and only held 3 subbasins (Figure 3-4).

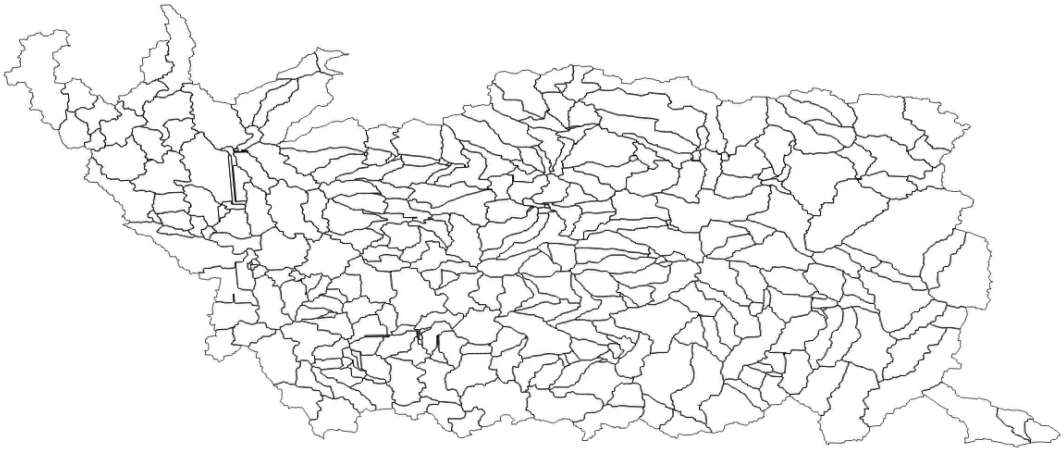

Figure 3-2: Subbasins - HUC8 polygons

3.5 Filter Modifications

The DHEnKF filter was implemented with a series of modifications that streamlined the filtering process.

3.5.1 Parameter Ranges

Parameter minimums and maximums were implemented on each model parameter to avoid anomalous or erratic model output such as negative snowfall or streamflow. The use of parameter bounds in Kalman filters is well researched and they have been used in a variety of past studies [33].

For every parameter θ a minimum θ_{min} and a maximum value θ_{max} was defined. If an ensemble member i was generated outside of the range (θ_{min}, θ_{max}) during the apriori phase it was adjusted to:

$$\theta^i = \begin{cases} \theta_{min} & \theta^i < \theta_{min} \\ \theta_{max} & \theta^i > \theta_{max} \end{cases} \tag{3.1}$$

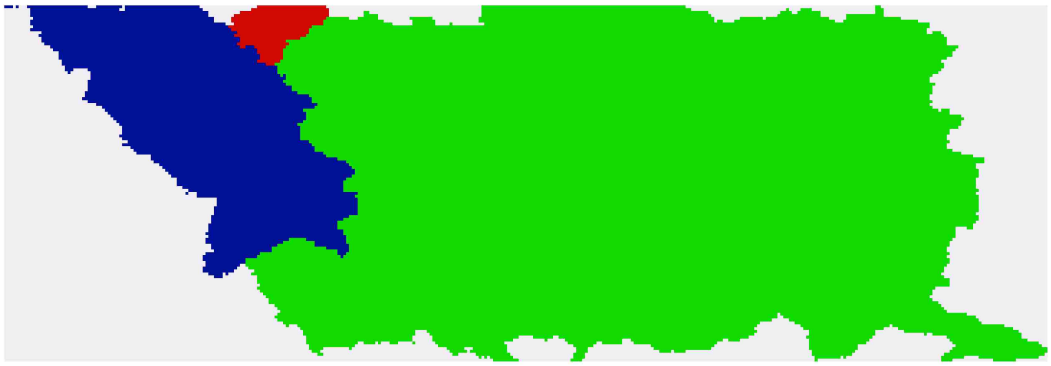

Figure 3-3: Montana's 3 HUC4 zones rendered onto the raster grid.

$$\theta^i = \begin{cases} \theta_{min} & \theta^i < \theta_{min} \\ \theta_{max} & \theta^i > \theta_{max} \end{cases} \tag{3.2}$$

For posterior parameters the same clipping logic from Eq. (3.2) is used. Initially an approach similar to the approach in [33] was utilized, but this logic kept parameters immobile when the innovation between the state and observations were very large, rendering the filter's parameter correction phase meaningless. To account for the problem of ensemble collapse, a minimum variance and a normalization feature was implemented (see below.)

3.5.2 Normalization Feature

To reduce erratic parameter ensemble behavior when sudden large discrepancies between observed data and model data appeared, a normalization feature was imple-

mented in the parameter correction phase. For every parameter θ a maximum movement range θ_{range} was defined based upon boundaries θ_{min} and θ_{max}. An empirical parameter γ controlled the maximum amount of movement per correction phase.

$$\theta_{range} = \gamma(\theta_{max} - \theta_{min}) \tag{3.3}$$

$\gamma = 1$ allows for unhindered movement for theta, while $\gamma = 0$ does not allow any movement. For the purposes of this paper $\gamma = .1$ greatly reduced filter instability while allowing parameters to converge relatively quickly to far away values.

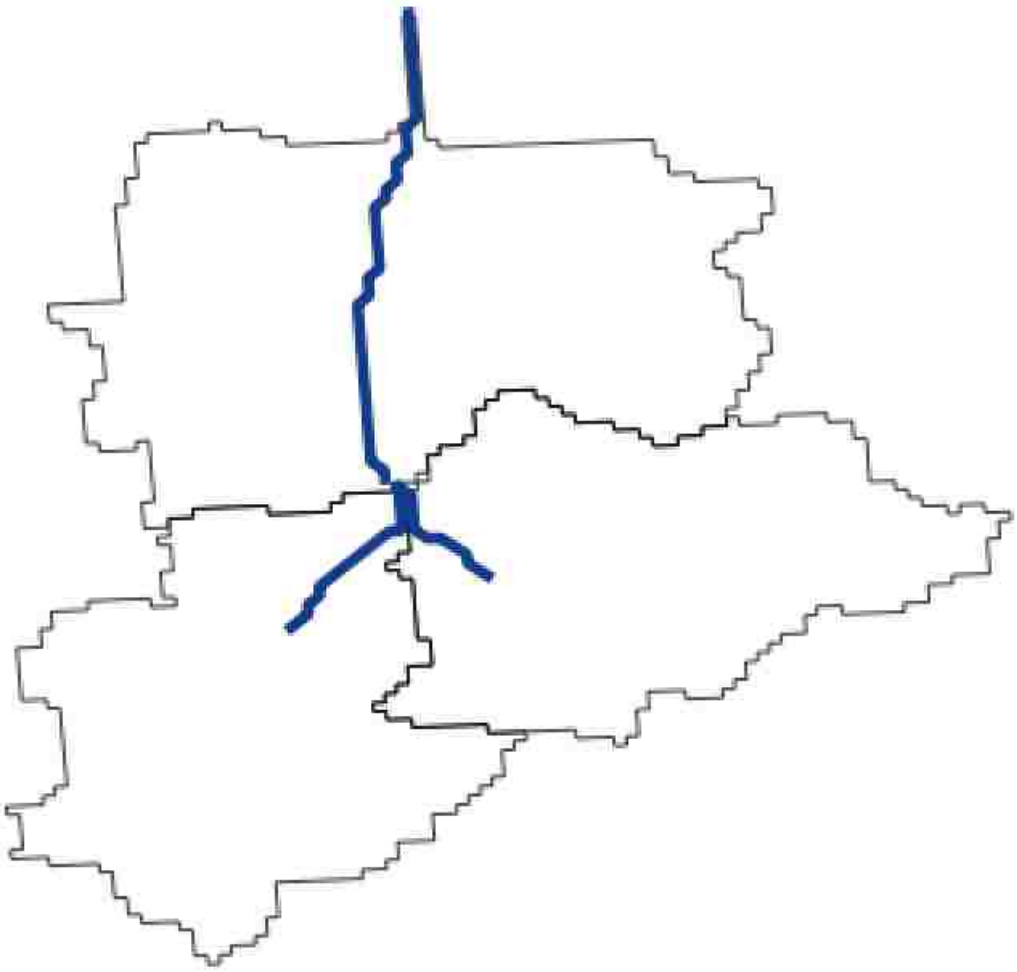

Figure 3-4: The small dataset's 3 subbasins and 3 streamreaches (blue).

Chapter 4

Results

4.1 Runtime Modifications: Perturation of States

Early attempts at running the DSHEnKF on the hydrologic model were marked by the complete collapse of posterior ensemble covariance to the mean and erratic jumps from the minimum to the maximum bounds for all streamflow parameters. Snow water equivalent parameters and states, however, converged in a stable fashion. It was determined that these erratic jumps were due to the hydrologic model's dependence on the value of the catchments' lowest groundwater reservoir, an unobserved and uncorrected state, which was integral to the production of streamflow in each timestep. White noise added to the forcing data (precipitation and min/max temperature) was unable to generate adequately diverse ensemble behavior when groundwater states were uniform across ensembles. To account for this, perturbation of groundwater and streamflow states was implemented.

4.1.1 Perturbation of Groundwater States

The hydrologic model was extremely sensitive to its starting states, in particular the lower groundwater reservoir. Underwhelming starting groundwater caused the parameters `ck0`, `ck1`, and `ck2` to converge towards values that emptied all water pouring into the reservoirs so modeled streamflow could match the observations. Conversely,

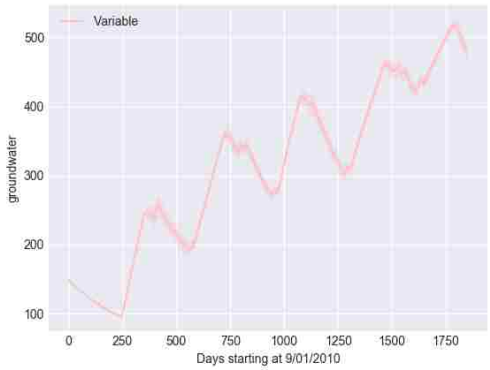

Figure 4-1: Uniform groundwater

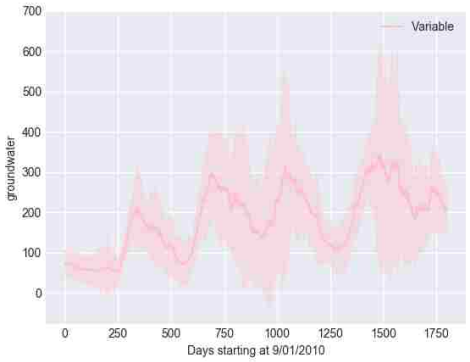

Figure 4-2: Perturbed groundwater

high starting groundwater caused `ck0`, `ck1`, and `ck2` to converge towards parameters that let very little groundwater out of the reservoirs, further exasperating the problem and causing higher and higher values for `ck0`, `ck1`, and `ck2` to be chosen.

To solve this issue and find a reliable blanket starting value for groundwater subcatchments in an efficient amount of time the small dataset was run using the parameter boundaries specified by [21]. Trial and error was utilized on the dataset until groundwater stabilized. To encourage the model to explore different parameter values for different amounts of groundwater, initial states for the large dataset were perturbed across all ensembles and catchments using a μ equal to the average stable value of the small dataset, which for this model was roughly calculated to be 100mm, and a σ of 80mm. During the prediction phase groundwater was treated as forcing data and was perturbed slightly at a σ of $u_{gw} * gw$, with $u_{gw} = .05$.

4.1.2 Continuous perturbation of streamflow and snow-water equivalent states

Another method of smoothing the model's calibration process despite its over-reliance on groundwater was through the direct perturbation of streamflow and swe states. This perturbation guaranteed that ensemble collapse was never fully realized. Gaussian noise was added to the state vector $\mathbf{x}_t^{i-}$ before the parameter correction state and the state correction stage such that

$$\mathbf{x}^{\mathbf{i-}}_{\mathbf{t,str}} + N(0, \mathbf{x}^{\mathbf{i-}}_{\mathbf{t,str}} \cdot -; pq_{str}) \tag{4.1}$$

and

$$\mathbf{x}^{\mathbf{i-}}_{\mathbf{t,swe}} + N(0, \mathbf{x}^{\mathbf{i-}}_{\mathbf{t,swe}} \cdot q_{swe}) \tag{4.2}$$

where q_{str} and q_{swe} are values between 0 and 1 representing model uncertainty. While the continuous perturation of streamflow and swe states was a useful debugging technique, large values for q_{str} and q_{swe} reduced the effectiveness of model calibration and were avoided.

4.2 Small dataset

To expedite the discovery of optimal initial values, errors, and minimum and maximum bounds for the complete dataset (see Table 4.1 and table 4.2) the small dataset was run and compared with the ranges proposed by [31] and [40] and then run again with boundaries optimized for the current model. The small dataset, which was comprised of 3 catchments around the Biterroot valley and consisted of one gauged catchment (henceforth referred to as catchment 241) and 2 ungauged catchments (catchments 244 and 248), was run over a period of 1095 days starting a little before Fall of 2010. Simulations began in September so modeled snowfall accumulation could be corrected first, allowing accurate snow melts to inform streamflow runoff in the Spring and Summer. All parameters in the small dataset converged to a set of values quickly but quickly readjusted when significant differences arose between the observed and modeled states.

4.2.1 Streamflow states and parameters

The gauged catchment 241's posterior streamflow state (leftmost graph in Figure 4-3) snapped to the observations quickly. Catchment 241's post-parameter corrected streamflow values (shown in yellow on the figures in 4-3) also closely followed the observations. Notice the slight discrepancy between the post parameter correction

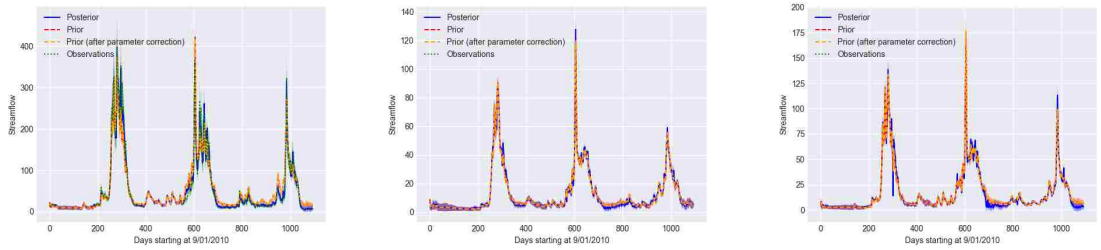

Figure 4-3: Streamflow states for the 3 small dataset catchments. From left to right: 241,244,248

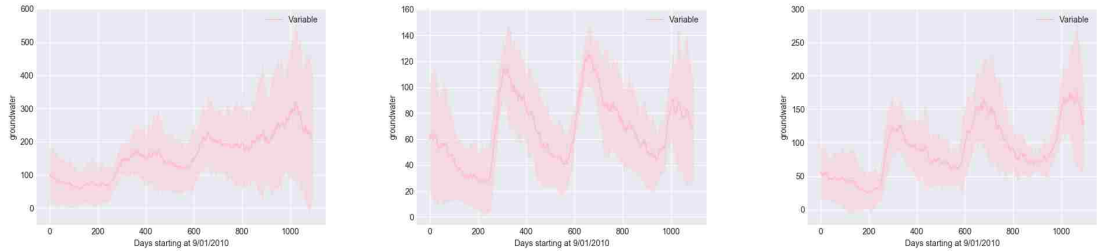

Figure 4-4: Groundwaters for the 3 catchments

state and posterior state seen in the first graph in Figure 4-3 during the Winter time periods. While state correction continuously tried to move streamflow down to a match the observed Winter state, parameters were not found that allowed streamflow to perfectly match the observed states. This behavior is connected to the value of the lower groundwater reservoir and is seen to some degree in the Winter months in almost all streamflow state graphs.

The lower groundwater reservoir in all three catchments rose 20mm-200mm throughout the 1095 day filtering period (Figure 4-4). Throughout this time the filter's values for `ck2` and `perc`, two parameters that impact the buildup and dispersion of lower groundwater, remained unchanged. The stabilization of the lower groundwater component in the hydrologic model is explored in Chapter 5.

As seen in the plots in Figure 4-7, parameter ensembles converged to the ensemble mean within the first 5-10 days and remained stable until the Spring and Summer months. When modeled results deviated significantly from observed states (and

Table 4.1: Hyperparameters - parameter perturbations and min/max ranges

Parameter (θ)	q	Min	Max
Degree Day Factor (`ddf`)	.75mm°C^{-1}d^{-1}	1mm°C^{-1}d^{-1}	8mm°C^{-1}d^{-1}
Tempature Threshold (`thres`)	.5°C	-2.5°C	2.5°C
Potential Evapo-Transpiration (`aet_lp`)	.15	.3	1
Ponded water to soil storage (`soil_beta`)	1.75	1	6
Soil compartment max capacity (`soil_max_wat`)	40	50mm	500mm
Immediate runoff (`ck0`)	6d^{-1}	.25d^{-1}	10d^{-1}
Fast runoff (`ck1`)	25d^{-1}	3.33d^{-1}	50d^{-1}
Groundwater runoff (`ck2`)	350d^{-1}	50d^{-1}	650d^{-1}
Groundwater water storage threshold (`hl1`)	25mm	0mm	50mm
Groundwater peculation (`perc`)	1.5d	3d	50d
Wave dispersion (`e`)	.35	.25	.4

therefore the innovation spiked) the ensemble increased in variance and its members searched for a more optimal value. This stair-stepping behavior is linked to the new hierarchical parameter perturbation algorithms and appears to be standard behavior for the DSHEnKF algorithm. The implications of this are explored in Chapter 5. Importantly, all catchment values remained unique and did not coverage to a spatial mean.

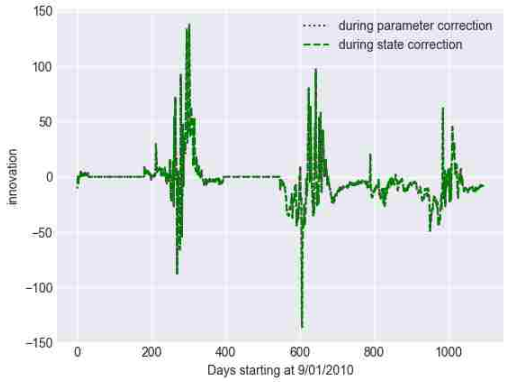

Figure 4-5: Streamflow innovation (catchment 241)

4.2.2 Snow-water equivalent states and parameters

Snow-water equivalent states and parameters behaved similarly to their streamflow counterparts. Catchment 241's snow-water equivalent states (Figure 4-8) snapped

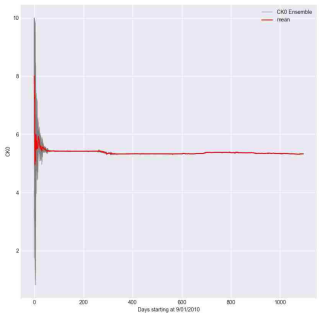

(a) 241:`ck0`

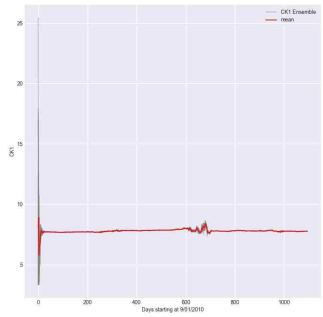

(b) 241:`ck1`

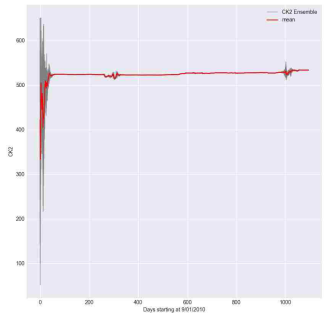

(c) 241:`ck2`

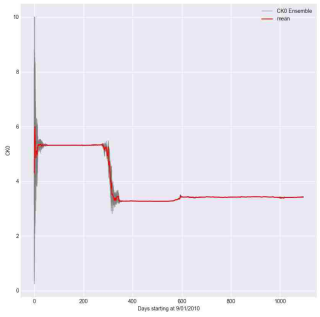

(d) 244:`ck0`

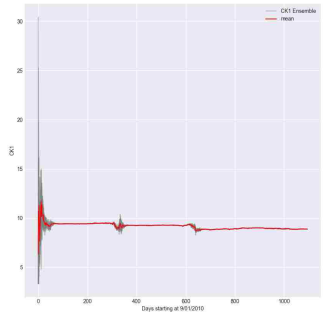

(e) 244:`ck1`

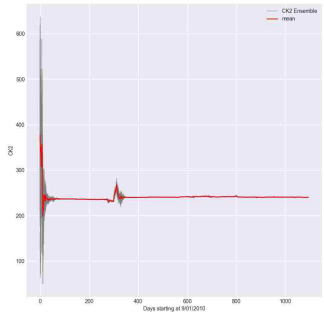

(f) 244:`ck2`

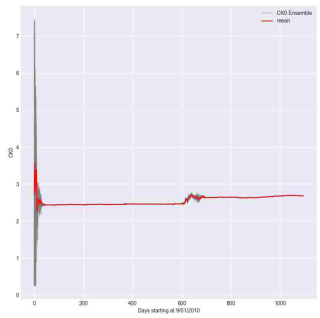

(g) 248:`ck0`

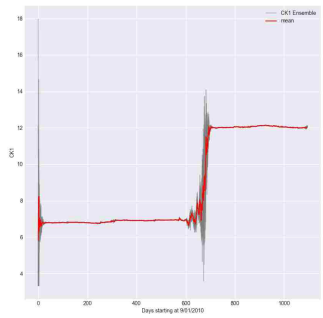

(h) 248:`ck1`

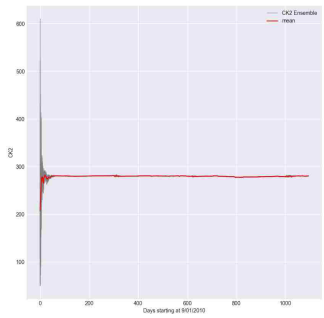

(i) 248:`ck2`

Figure 4-7: Convergence of `ck` parameters for all 3 catchments

Table 4.2: Initial parameter values

Parameter (θ)	Starting Value
Degree Day Factor (`ddf`)	.4mm°C^{-1}d^{-1}
Tempature Threshold (`thres`)	2°C
Potential Evapo-Transpiration (`aet_lp`)	.5
Ponded water to soil storage (`soil_beta`)	4.8
Soil compartment max capacity (`soil_max_wat`)	400mm
Immediate runoff (`ck0`)	20d^{-1}
Fast runoff (`ck1`)	200d^{-1}
Groundwater runoff (`ck2`)	300d^{-1}
Groundwater water storage threshold (`hl1`)	20mm
Groundwater peculation (`perc`)	10d
Wave dispersion (`e`)	.37

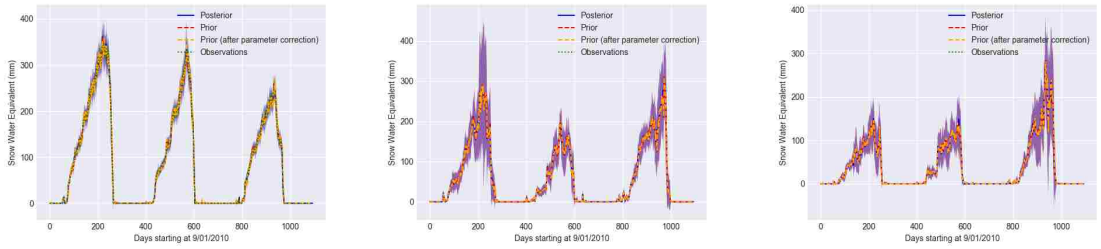

Figure 4-8: Snow-water equivalent states for the 3 catchments. From left to right: 241, 244, 248

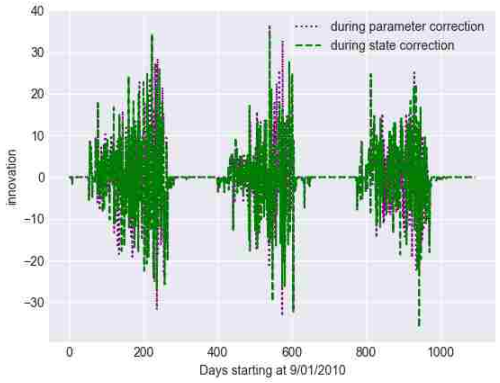

Figure 4-9: SWE innovation (catchment 241)

to the observations quickly. Snow-water equivalent innovation (Figure 4-9) is somewhat less biased then streamflow innovation (Figure 4-5). Snow-water equivalent parameters behaved similarly to their streamflow counterparts. All ensembles and catchments converged to ensemble means within the first 20 days and did not significantly deviate from their chosen values throughout the remainder of calibration (Figure 4-11.) Similarly to the streamflow parameter ensembles, each catchment's value remained unique and did not converge to the mean (more easily seen in Figure 4-13.)

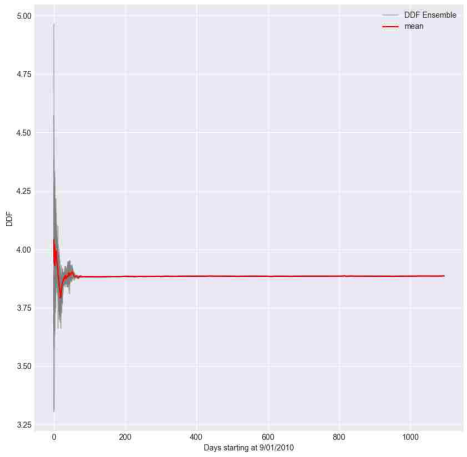

(a) 241:`ddf`

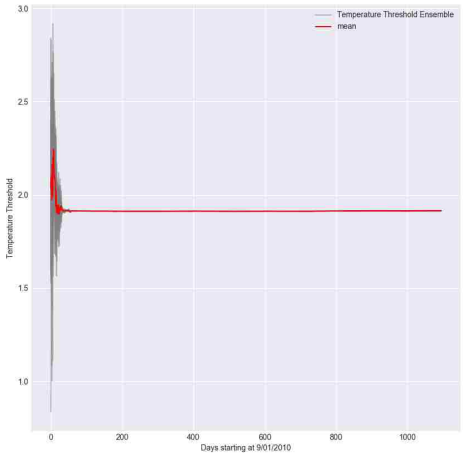

(b) 241:`thres`

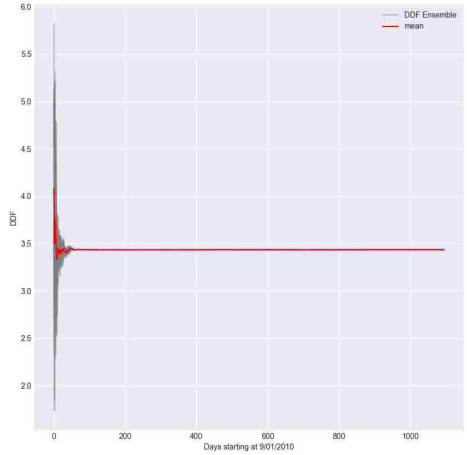

(c) 244:`ddf`

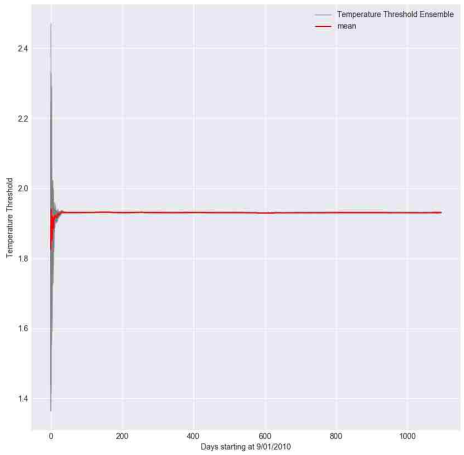

(d) 244:`thres`

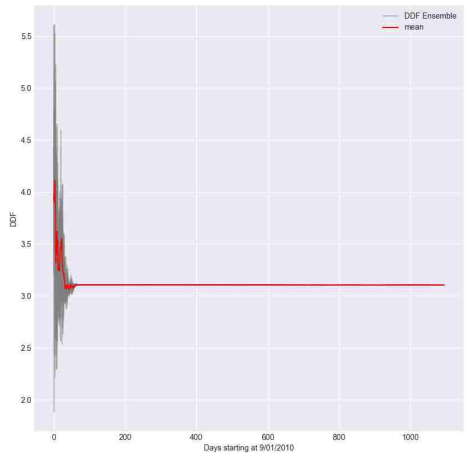

(e) 248:`ddf`

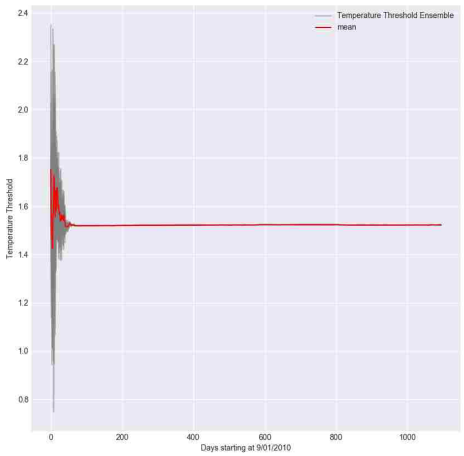

(f) 248:`thres`

Figure 4-11: Convergence of `ddf` and `thres` parameters for all 3 catchments

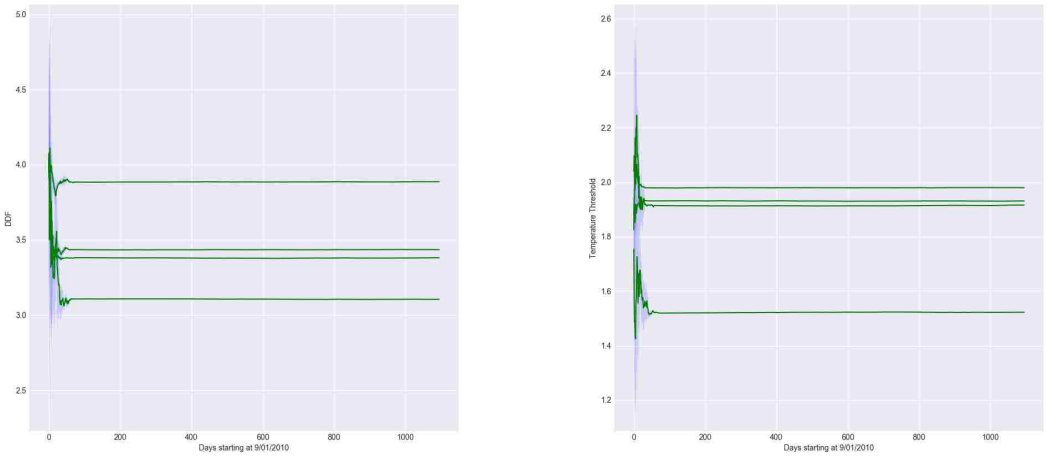

(a) All catchments:`ddf` (b) All catchments:`pp`

Figure 4-13: All SWE parameters stabilized quickly during the run of the small dataset. `a` = .9

4.3 Complete Dataset

After workable initial values, errors, and boundaries and had been selected the complete dataset was calibrated. Calibration of the complete dataset was computationally expensive and a balance had to be struck between ensemble size, time run, and data collected per timestep. For these results a full three years (1095 days) was run with 100 ensemble members. The effects of different ensemble sizes on results is discussed in Chapter 5. Running the DSHEnKF on the large dataset produced good results that point to both strengths in the hierarchical design and further research opportunities.

4.3.1 Streamflow states and parameters

Streamflow calibration on the complete dataset progressed in a similar way to calibration on the small dataset, but more variation in geographic location helped identify patterns in the DSHEnKF method. All parameters in individual watersheds collapsed to their means in the first 30 days and increased in variance when large discrepancies existed between modeled behavior and observed streamflow behavior. While gauged posterior states matched their observations, innovation tended to be biased in either

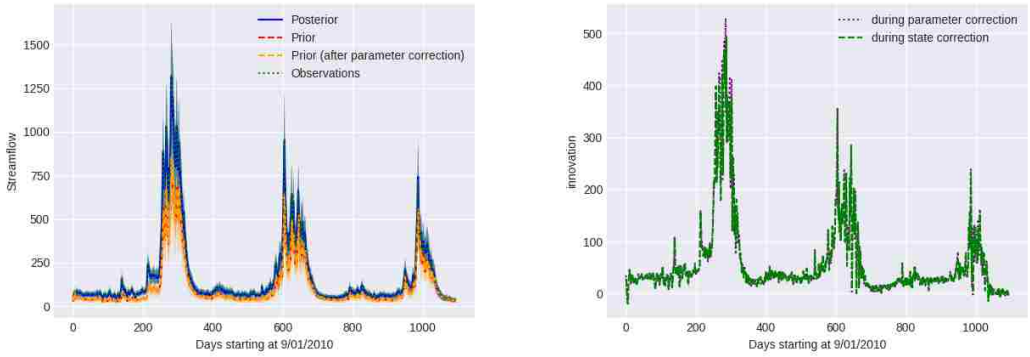

Figure 4-14: A gauged streamflow state (catchment 198) and its innovation

the positive or the negative direction (Figure 4-14.) It is believed that this is primarily due to the model's heavy dependence on groundwater to influence a timestep's state as discussed in section section 4.1.

Streamflow parameters converged in a similar fashion to the small dataset's parameters (Figure 4-16.) Note how the ensembles tend to reconstitute during the Spring and Summer time periods - this is most noticeable in the `ck0` graph in 4-17. Patterns in the distribution of streamflow parameters are explored in Chapter 5.

4.3.2 Snow-water equivalent states and parameters

Snow-water equivalent calibration on the complete dataset behaved similarly to streamflow calibration.

Figure 4-22 shows the traces for the `ddf` and `pp` parameters. These parameters remained locked at their chosen values after the 100th time step. States converged to the observations quickly in gauged nodes (Figure 4-18 and innovation was generally unbiased (Figure 4-19.)

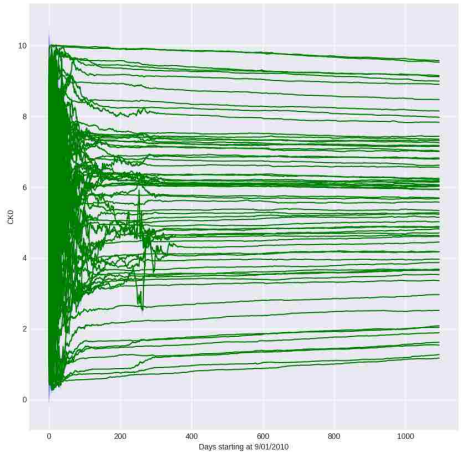

(a) `ck0`

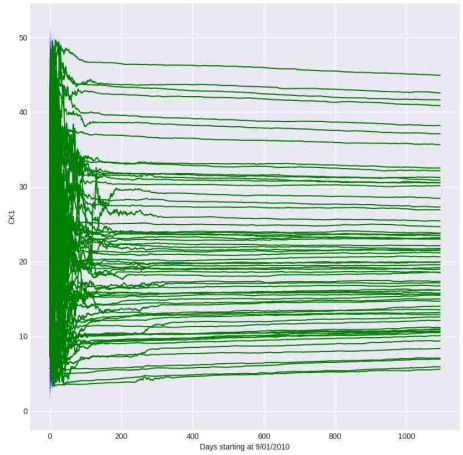

(b) `ck1`

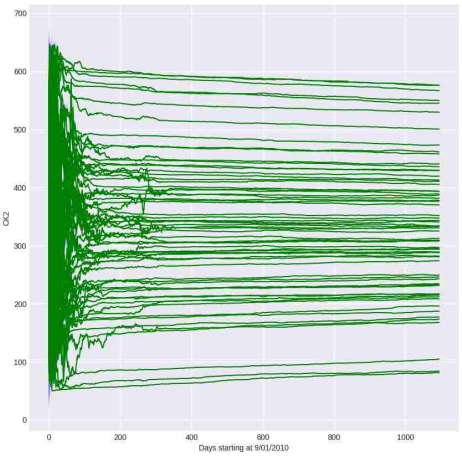

(c) `ck2`

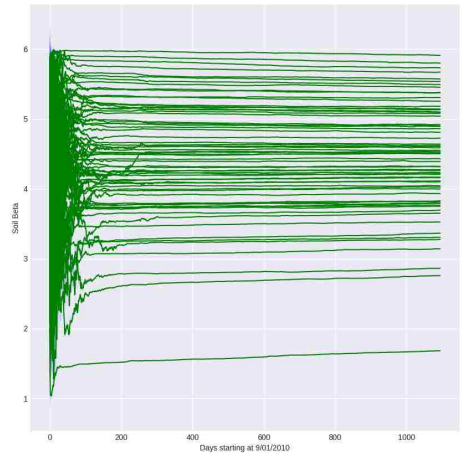

(d) `soil_beta`

Figure 4-16: All streamflow catchments converged quickly to specific values.

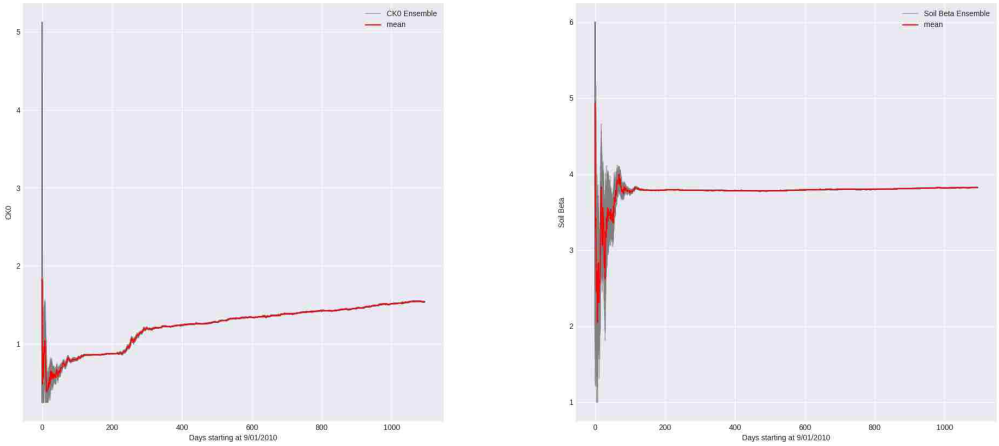

Figure 4-17: Traces for catchment 198 - `ck0` and `soil_beta`

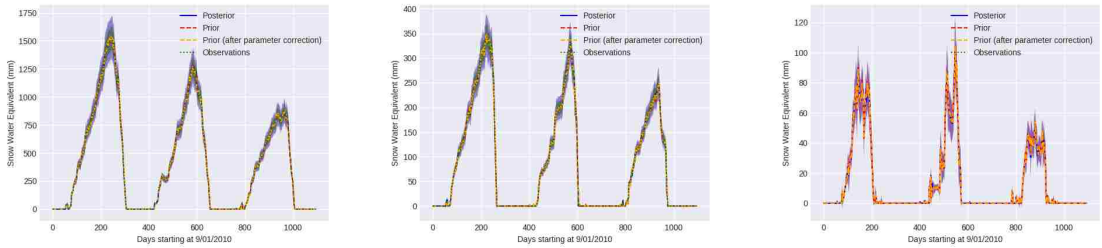

Figure 4-18: Snow-water equivalent states for 3 catchments: 42 (gauged), 241 (gauged), and 137 (ungauged)

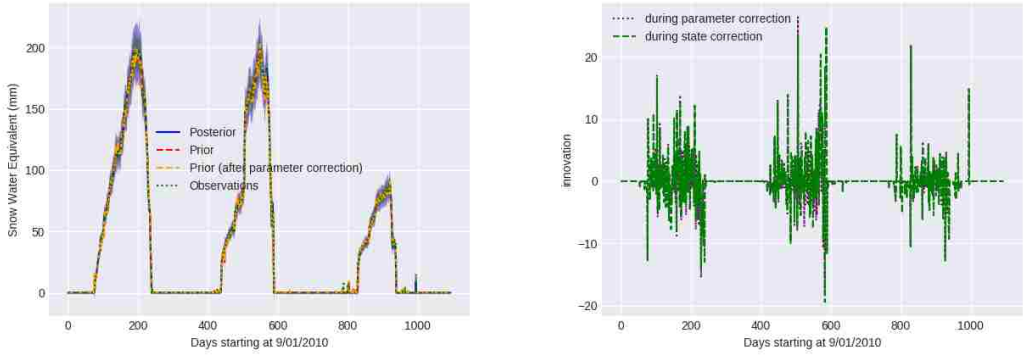

Figure 4-19: A gauged swe state and its innovation (catchment 170)

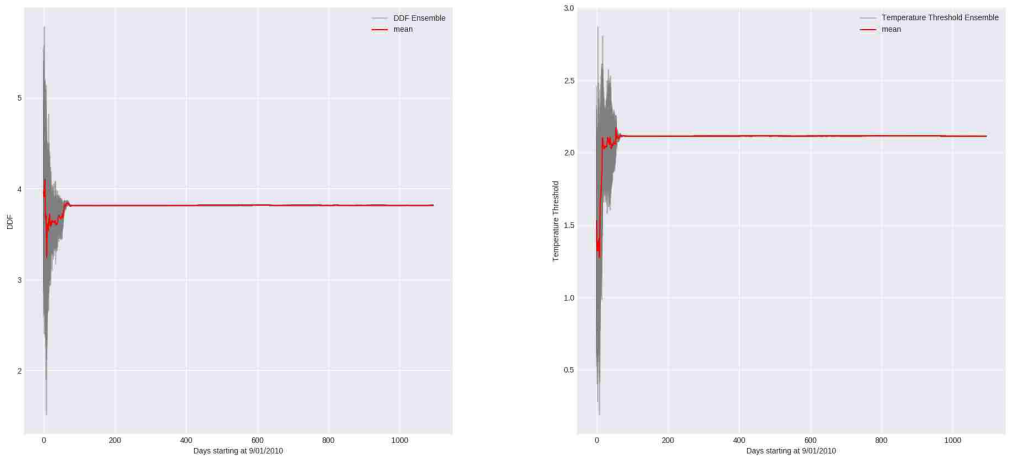

Figure 4-20: ddf and temperature threshold - catchment 170

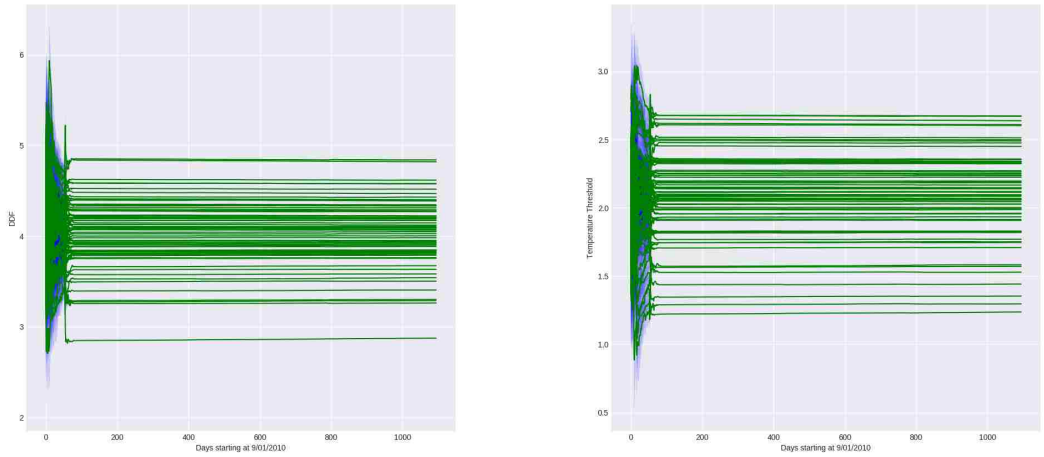

(a) `ddf` (b) `pp`

Figure 4-22: All traces of snow water equivalent related parameters

4.4 Effects of the Hierarchical Blending Component

To observe the effects of the hierarchical component on the filtering process the small dataset was run over 365 timesteps with different values for `a`. The difference in parameter traces for different values of `a` may be seen in Figure 4-24. The value of `a` controls the maximum amount of weight that may be given to the group mean when ensemble variance as $\lim var(\theta) \rightarrow \infty$. A very low to nonexistent `a` value would allow no transfer of data between catchments, while a high `a` value allows for a complete transfer of information at the expense of temporal memory. For the hydrologic model it was decided that the filter seeks parameters best when `a` = .9.

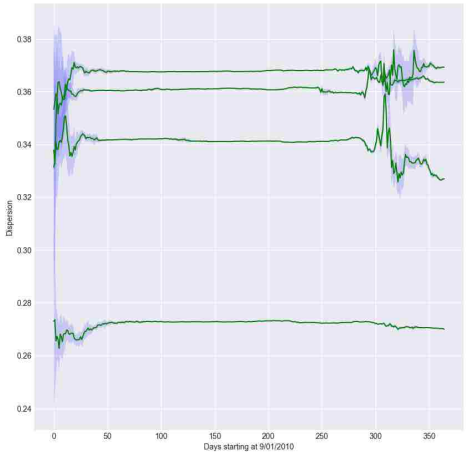

(a) a = .1

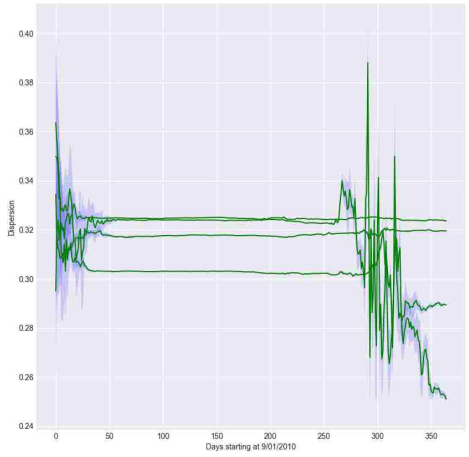

(b) a = .4

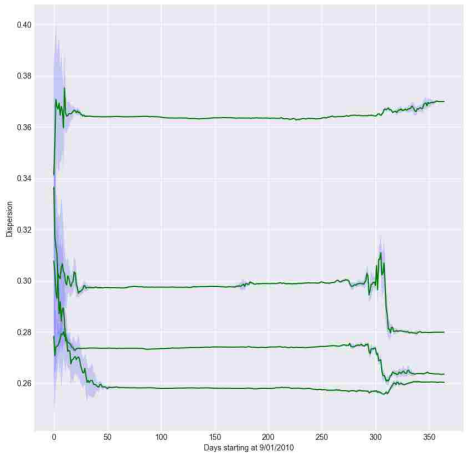

(c) a = .65

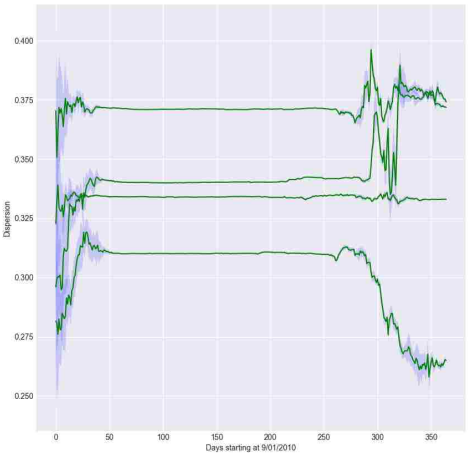

(d) a = .99

Figure 4-24: Effect of different values for the blending component a

Chapter 5

Analysis, Further Research Opportunities and Conclusion

5.1 Analysis

5.1.1 The Significance of Ensemble Size

To observe the effect of ensemble size on the DSHEnKF filtering process, a 50 ensemble run and a 25 ensemble run were compared to the 100 ensemble run from chapter 4. The 50 ensemble and 25 ensemble run were identical to the 100 ensemble run in regards to starting parameters. Figure 5-1 shows how streamflow estimations for an ungaged catchment in the filtering process evolve as more ensembles are added. As the leftmost graph demonstrates, small numbers of ensembles lead to spurious streamflow predictions in both the prior and posterior. However, as demonstrated in Figure 5-2, this spurious behavior does not translate into the unfiltered run of the model. Figures 5-2 and 5-4 demonstrate how the model performs when utilizing the unfiltered 50 ensemble and 100 ensemble parameters.

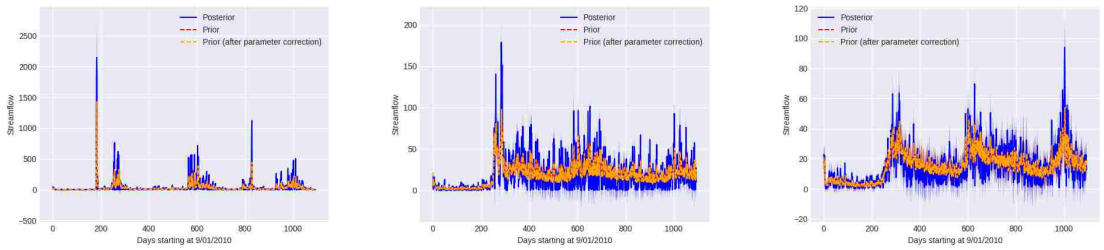

Figure 5-1: Streamflow states for ungaged catchment 194 during the filtering process. From left to right: 25 ensembles, 50 ensembles, 100 ensembles

5.1.2 Comparison of Filtered Parameters

To analyze the accuracy of the Dual State Hierarchical Ensemble Kalman Filtering algorithm, the final calibrated parameter values were taken from Chapter 4's run and applied to a standard unfiltered hydrologic model. The model was run over a period of 6 years and the results were compared to a run of the hydrologic model with the initial parameters from Table 4.2, the 50 ensemble run mentioned earlier in this chapter, and the corresponding gauged catchments. Figure 5-4 shows the varying results from 4 catchments. Catchments 115 and 173 show a clear improvement over the initial modeled results. Catchment 173 demonstrates the danger of using an inferior number of ensemble members, as the initial estimates are superior to the 50 ensemble run. Catchment 139 demonstrates a case where the filtered parameters were unable to successfully emulate the observed state. Overall, the filtered parameters represent an improvement over the non-filtered parameters when compared to the observed states.

5.1.3 Groundwater Accumulation Process and Correlated Parameters

While both the 50 ensemble run and 100 ensemble run of the model generally produced reasonably accurate streamflow estimates, many parameters, particularly the groundwater parameters `ck2` and `perc`, tended to differ greatly in spatial distribution. This warranted an evaluation of these parameter's correlation, the results of which

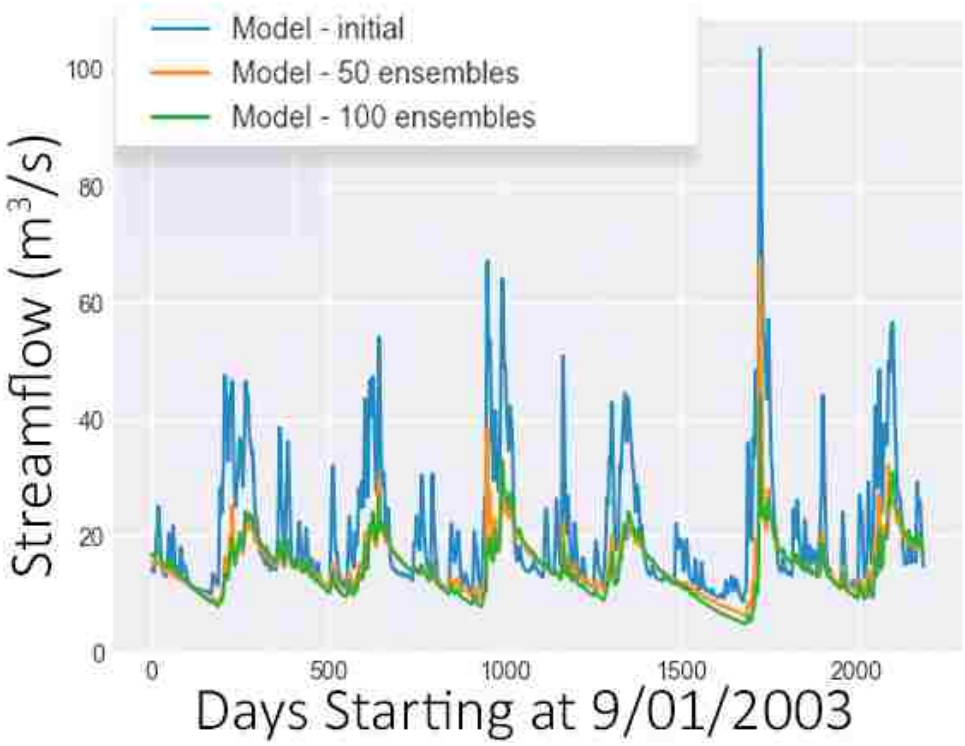

Figure 5-2: The resulting hyrdologic model run over 6 years for the ungaged catchment 194 from Figure 5-1

can be seen in figure 5-5. `ck2` was determined to be inversely proportional to `perc`. Therefore, while these two parameters were calibrated in such a way that groundwater remained stable, different amounts of groundwater are collected and dispersed in the lower reservoir (Figure 5-9). Therefore, while the DSHEnKF placed all parameters in reasonable positions in both runs, the correlated nature of these and other parameters can result in different distributions of parameters. Correlated parameters have been documented in HBV models in the past [15], [23], [21] and as a result these results are not surprising. Final parameters may be expected to lock onto different parameter values per each filtering run and potentially cause ungauged outputs like groundwater to differ.

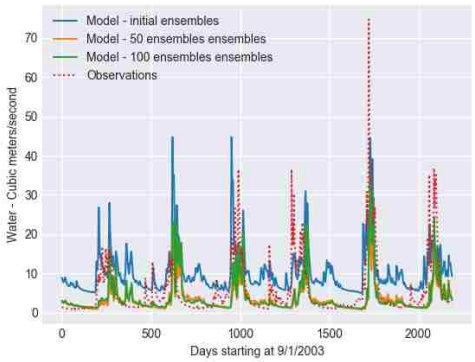

(a) Catchment 115

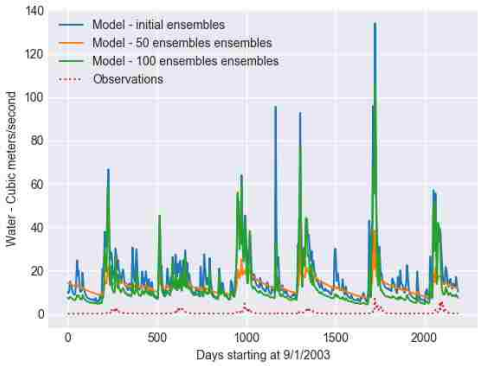

(b) Catchment 139

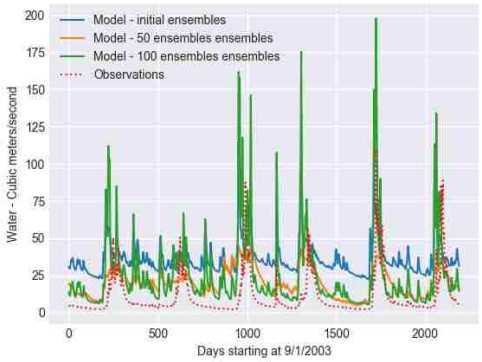

(c) Catchment 165

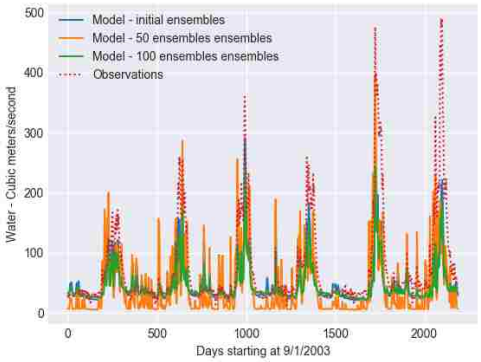

(d) Catchment 173

Figure 5-4: 4 runs of the hydrologic model compared to the observed state: initial parameters from Table 4.2, parameters from a 50 ensemble run, parameters from a 100 ensemble run.

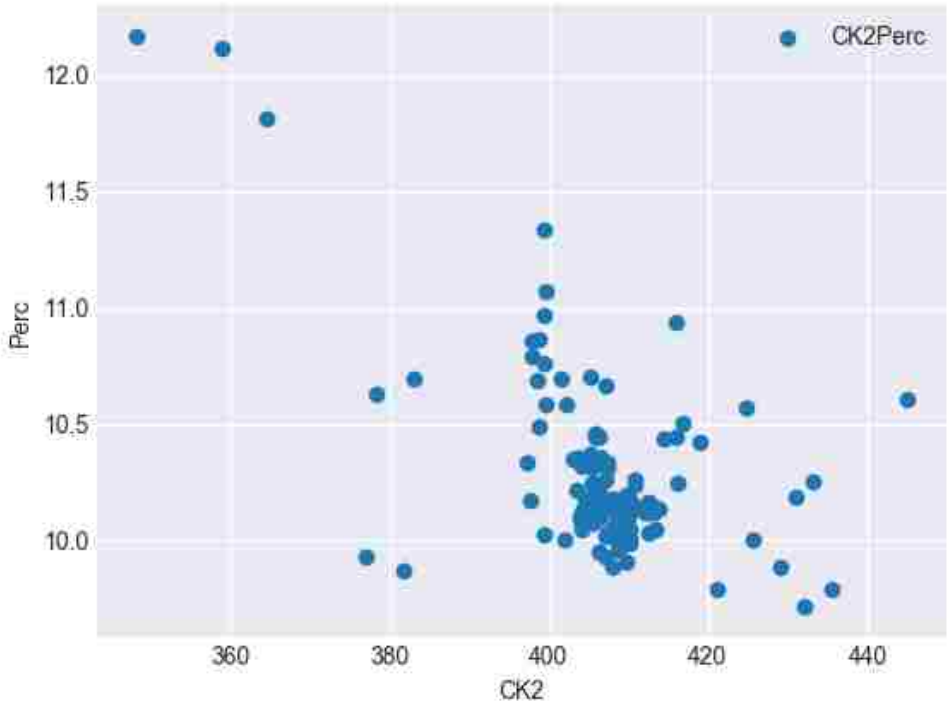

Figure 5-5: `perc` values plotted against ck2 values.

5.1.4 Ensemble Variance

While the Dual State Hierarchical Ensemble Kalman Filtering algorithm possesses many of the same characteristics as the standard Dual State Ensemble Kalman Filtering algorithm developed by Moradkhani et. al in 2005 [26], there are some important differences. One of of the largest differences is the DSHenKF's ensembles' tendency to rapidly collapse to the ensemble mean after the mean locks onto a working parameter value. In a standard Ensemble Kalman Filter this variance collapse would be an unwanted effect because the variance between ensembles is a measure of the uncertainty in a parameter. However, the nature of the new hierarchical parameter perturbation scheme encourages this behavior through its dynamic weighting of the ensemble mean as ensembles converge. A large variance in ensemble size, in fact, would indicate a larger reliance on the group mean and would indicate the parameter has not yet found a suitable value (see figure 5-10 for an example of this.) Con-

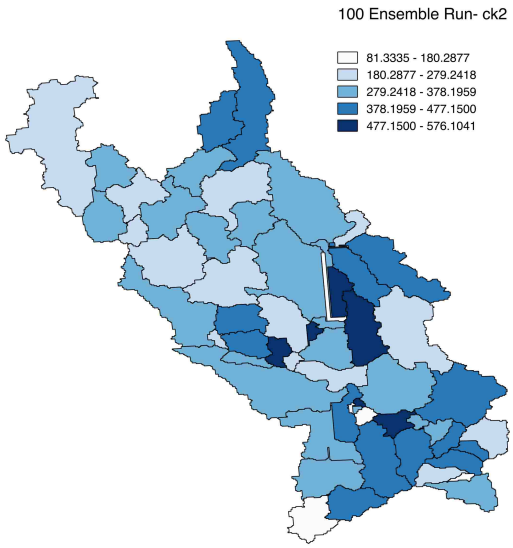

(a) 100 ensemble run: `ck2`

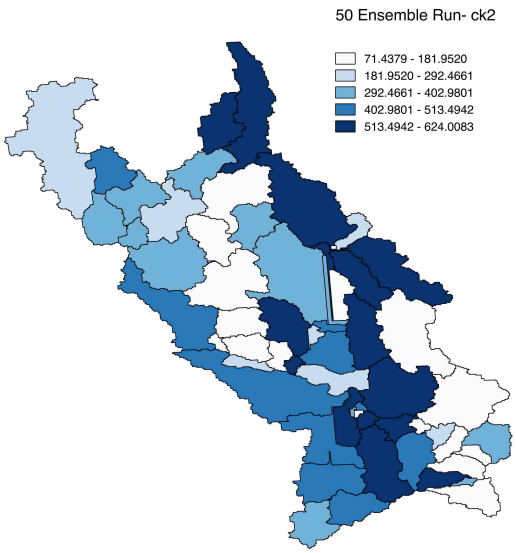

(b) 50 ensemble run: `ck2`

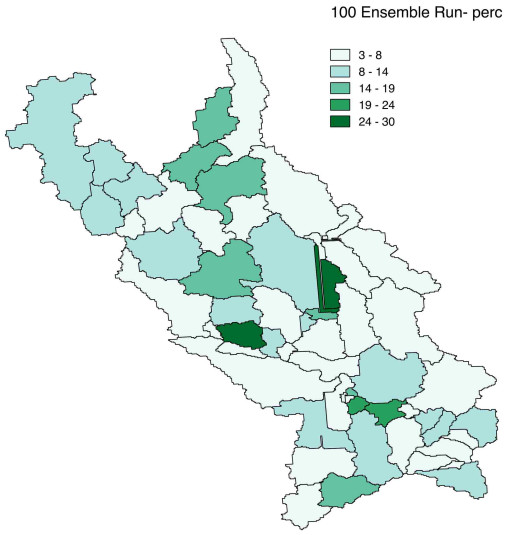

(c) 100 ensemble run: `perc`

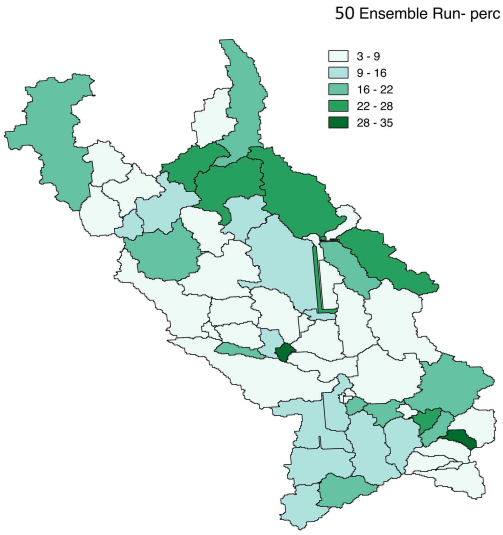

(d) 50 ensemble run: `perc`

Figure 5-7: Final parameter distributions for the 50 and 100 ensemble runs of the complete dataset

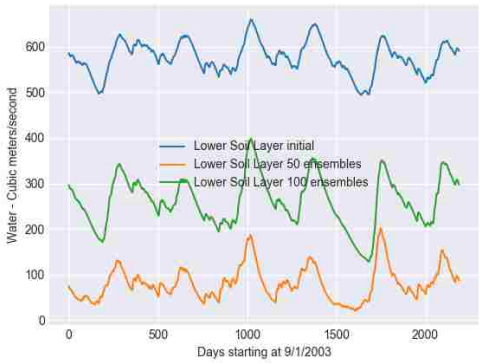

(a) Catchment 115

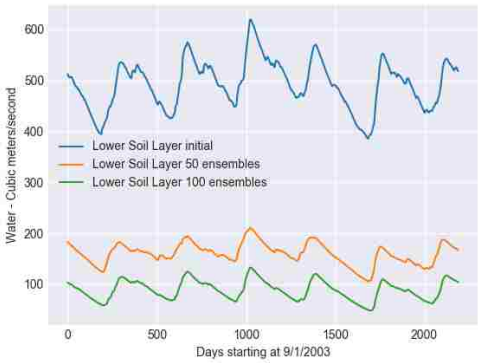

(b) Catchment 139

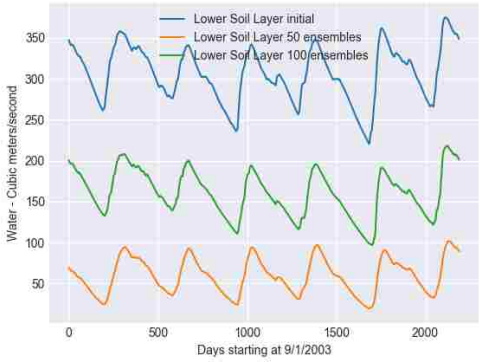

(c) Catchment 165

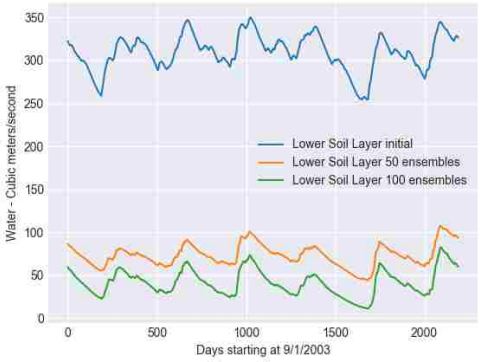

(d) Catchment 173

Figure 5-9: Lower groundwater reservoir water levels from the runs in Figure 5-4

sequently, the uncertainty in an ensemble of parameters in the DSHEnKF method is not necessarily a sign of the lack of variance in a parameter and may simply be the result of a calibrated ensemble of parameters or dormant ensemble of parameters that will reconstitute as soon as the value of the parameter becomes relevant to the model's tracking of the observations.

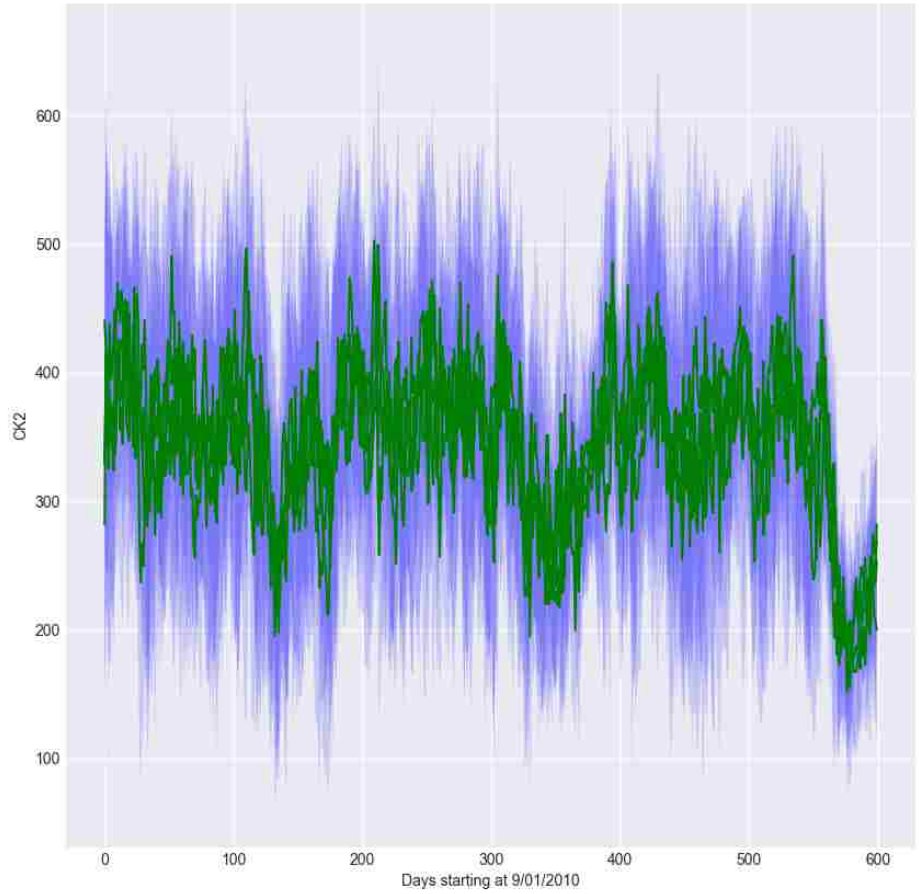

Figure 5-10: An example of a parameter's behavior when it is unable to lock onto a a set of values. In this case, this parameter cannot lock because `b` is too large.

5.2 Further Research Opportunities

This research introduces and explores the potency of the DSHEnKF method. However, research must be done to compare the accuracy and efficiency of the DSHEnKF method to other filtering algorithms such as the vanilla Dual-State Ensemble Kalman Filter, the Particle Filter, the Joint Ensemble Kalman Filter, and the Unscented Kalman Filter.

Due to computational limitations, certain tests and comparisons such as the optimal ensemble size for the DSHEnKF, the filtering of very large datasets over large time periods, experimentation with multiple hierarchical groupings, or the expansion of state correction to other outputs of the hydrologic model such as groundwater were not attempted. Further research using a different model or more capable computer would flesh out the advantages and disadvantages of the DSHEnKF method.

As discussed in subsection 5.1.4, ensemble variance collapses quickly in this method. The advantages and disadvantages of this effect should be explored. The exploration of the calculation of the b parameter in the dynamic alpha equation is integral to optimizing this issue since b controls the variance at which the hierarchically generated vector of parameters begins to be mixed with the mean of the parameters. In addition to new methods of calculating b, the testing of new ways of determining α apart from the logistical formula suggested here is also warranted.

Since this study introduced the methodology and results of the DSHEnKF and utilized observed catchments to determine the algorithm's usefulness, further research into the accuracy of the DSHEnKF's ability to calibrate ungaged catchments through its hierarchical component is warranted. The ability to calibrate these ungaged catchments is one of the DSKEnKF's most important applications in the realm of hydrologic modeling.

5.3 Summary

The DSHEnKF method has been proven to be a useful calibration procedure on hierarchically structured datasets, and it has been determined that the DSKEnKF can successfully filter parameters and states and that the final filtered parameters produce more accurate results. A Dual State Hierarchical Ensemble Kalman Filter was chosen to calibrate the hydrologic model because 1) the DSHEnKF does not have to compute the high dimensional state covariance matrix during the update phase as the ensemble covariance matrix may be substituted in its place, 2) the hydrologic model is a sequential model that could conceivably benefit from real-time parameter correction, and 3) 10+ years of observed streamflow and SWE data may be compared to model data to test for over-fitting. While the potential applications of the DSKEnKF are exciting, further research is needed to understand this method's usefulness when compared to other filtering methods.

Appendix A

The Hydrologic Model

This model is a hydrologic system that couples a rainfall-runoff model to a routing component that simulates streamflows within a regional stream network. An HBV model [5, 6] was modified to simulate hydrologic processes like snowmelt, evapotranspiration, and infiltration at the subcatchment level and transform the resulting precipitation into runoff and streamflow. This streamflow is then routed via the Muskingum-Cunge routing algorithm [9]. Below is a description of the implementation of those algorithms.

A.0.1 Rainfall Runoff component

The HBV model [5, 6] contains a mixture of raster-based and vector-based operations. Raster-based operations utilize spatially distributed data drawn from meteorological databases (precipitation and temperature data.) The raster grid is also used to calculate snow accumulation, melt, and soil processes. These are informed both by input from the meteorological databases and by a series of spatially distributed parameters, such as potential evapotranspiration. Vector-based operations increase computational efficiency through the use of polygons. Unique polygons are indexed by k later in this appendix while grid points are indexed by j. Uniform hydrologic response units (HRUs) are implemented to aggregate runoff production over these polygons and thus act as the bridge between the vector based operations and raster

Table A.1: Hydrologic Model Outputs - Raster or Vector

Name	Category
Snow Water Equivalent	Raster
Evapo-Transpiration	Raster
Snow Melt	Raster
Pond	Raster
Soil Moisture	Raster
Upper Soil Storage	Vector
Lower Soil Storage	Vector
Runoff	Vector

Table A.2: Hydrologic Model Parameters - Raster or Vector

Name	Purpose	Type
`ddf`	Degree Day Factor	Raster
`thres`	Temperature Threshold	Raster
`aet_lp`	Potential Evapo-Transpiration	Raster
`soil_beta`	Portion of ponded water that goes into soil storage	Raster
`soil_max_wat`	Soil compartment maximum water capacity	Raster
`ck0`	Immediate runoff	Vector
`ck1`	Fast runoff	Vector
`ck2`	Groundwater runoff	Vector
`hl1`	Groundwater water storage threshold	Vector
`perc`	Groundwater peculation	Vector
`K`	Wave celerity	Vector
`e`	Wave dispersion	Vector

based output. Table A.1 categorizes each model output as a vector based (one value per polygon) or raster-based (one value per pixel) output, while Table A.2 does the same for parameters.

Precipitation/Snowpack To determine the amount of precipitation that becomes snowfall and which amount becomes rainfall, minimum and maximum temperature data are compared to a critical temperature threshold Tc.

$$Snow_j^t = \begin{cases} P_j^t & Tmax_j^t < Tc_j \\ P_j^t * \frac{Tc_j - Tmin_j^t}{Tmax_j^t - Tmin_j^t} & Tmin_j^t < Tc_j < Tmax_j^t \\ 0 & Tmin_j^t > Tc_j \end{cases} \tag{A.1}$$

$$Rain_j^t = P_j^t - Snow_j^t \tag{A.2}$$

Where variables and parameters with a subscript j are spatially distributed and are at unique gridpoint j and variables and parameters with a superscript t are time-dynamic. P is precipitation ($\mathrm{mm\,d^{-1}}$), $Tmax$ is maximum air temperature (°C), $Tmin$ is minimum air temperature, $Snow$ is precipitation as snowfall ($\mathrm{mm\,d^{-1}}$), and $Rain$ is liquid precipitation. Any snowfall during one day t contributes to the snowpack's snow water equivalent (SWE, (mm)):

$$SWE_i^t = SWE_i^{t-1} + Snow_j^t \Delta t \tag{A.3}$$

A degree day model is utilized to simulate snowpack melt. Snowpack begins to melt when the average air temperature exceeds air temperature threshold Tm.

$$Melt_j^t = ddf_j * (Tav_j^t - Tm_j)] \text{ for } Tav_j^t > Tm_j \tag{A.4}$$

$$Rain_j^t = P_j^t - Snow_j^t \tag{A.5}$$

Where $Melt$ represents water released from the snowpack ($\mathrm{mm\,d^{-1}}$), Tav is average air temperature over the time step (°C), and ddf is the degree day factor ($\mathrm{mm\,d^{-1}\,{}^{\circ}C^{-1}}$). ddf is an empirical parameter controlling the snowmelt rate per degree of air temperature above temperature threshold Tm.

Melt from the snowpack at time t is subtracted from the snowpack and added to the amount of ponded water:

$$Pond_j^t = Pond_j^{t-1} + (Melt_j^t + Rain_j^t)\Delta t \tag{A.6}$$

$$SWE_j^t = SWE_j^t - Melt_j^t \Delta t \tag{A.7}$$

Where $Pond$ (mm) represents liquid water ponding at the surface.

Soil processes Ponded water infiltrates into the soil and is either placed in the soil system or is added to the topsoil compartment where it generates speedy runoff. The fraction of ponded water that infiltrates is an exponential function of the relative water storage already in the soil:

$$\Delta SM_j^t = Pond_j^t * \left(1 - \frac{SM_j^t}{FC_j^t}\right)^{\beta} \tag{A.8}$$

$$\tag{A.9}$$

where SM (mm) is the amount of water in the soil compartment and FC (mm) is the maximum capacity of water the soil compartment can hold before water begins percolating to the groundwater system. *beta* (dimensionless) is an empirical parameter. Actual evapotranspiration (AET, $\mathrm{mm\,d^{-1}}$) is calculated at the same time. Actual evapotranspiration reduces the amount of water storage in the soil and, just like ΔSM_j^t, is informed by the degree of saturation in the soil (SM over FC).

$$AET_j^t = PET_j^t * \left(\frac{SM_j^t}{FC_j * LP_j}\right)^{l} \tag{A.10}$$

$$\tag{A.11}$$

where PET is potential evapotranspiration ($\mathrm{mm\,d^{-1}}$)) and l (dimensionless) is an empirical parameter. Soil water storage dynamics and the amount of surface water that generates fast runoff are controlled by infiltration and actual evapotranspiration:

$$SM_j^t = SM_j^t + \Delta SM_j^t - AET_j^t \Delta t \tag{A.12}$$

$$OVL_j^t = Pond_j^t - \Delta SM_j^t \tag{A.13}$$

where OVL (mm) represents water that recharges the near-surface runoff-generating compartment.

Groundwater Compartments and runoff generation The groundwater system is comprised of two ground-water compartments that generate outflow. The top compartment's outflow represents both immediate runoff, which joins runoff in the current timestep, and fast runoff, which joins runoff through the runoff rates $Q0$ and $Q1$. The lower compartment's outflow represents baseflow. These processes are performed at the HRU level, which means overland flow and soil moisture values, both of which are represented over the raster grid, are averaged over overlaid polygonal subwatersheds representing HRUs. Spatial arithmetic that averages soil water storage over all grid cells j contained within a given polygonal HRU k is indicated by angle brackets $< . >$. The mass balance and percolation of water from the upper to the lower compartment of the groundwater system is implemented as:

$$Rech_k^t =< OVL_j^t >_k + < max(SM_j^t - FC_j, 0) >_k \tag{A.14}$$

$$SUZ_k^t = SUZ_k^{t-1} + Rech_k^t + Pond_k^t - Q0_k^t \Delta t - Q1_k \Delta t - PERC_k \tag{A.15}$$

$$SLZ_k^t = SLZ_k^{t-1} + PERC_k - Q2\Delta t \tag{A.16}$$

$Rech$ (mm) represents water storage in the fast runoff generating near-surface compartment, SUZ (mm) represents the storage in the upper groundwater compartment, and SLZ (mm) represents water storage in the lower groundwater compartment in HRU k at time step t. $Q0$, $Q1$, and $Q2$ ($\mathrm{mm\,d^{-1}}$) are each unique runoff rates. $Q0$ represents the soil surface runoff rate, $Q1$ represents the upper soil compartment runoff

rate, and $Q2$ lower soil compartment runoff rate. These are calculated as follows:

$$Q0_k^t = max((SUZ_k - HL1_k) * \frac{1}{CK0_k}, 0.0) \tag{A.17}$$

$$Q1_k^t = SUZ_k * \frac{1}{CK1_k} \tag{A.18}$$

$$Q2_k^t = SLZ_k * \frac{1}{CK2_k} \tag{A.19}$$

$$Qall_k^t = Q0_k^t + Q1_k^t + Q2_k^t \tag{A.20}$$

$HL1$ (mm) is an empirical parameter controlling a water storage threshold that triggers the generation of fast runoff. $CK0$, $CK1$, and $CK2$ (d) are empirical parameters that represent the characteristic drainage times of the soil surface, upper compartment, and lower compartment respectively.

Total outflow from any given HRU k on day t is distributed over time in order to produce the catchment response. This is accomplished through the convolution the output of HRU k by triangular standard unit hydrograph with base M_{base}.

$$Q_j^t = \sum_{i=1}^{M_{base}} Qall_j^{t-i+1} U(i) \tag{A.21}$$

$$U(i) = \begin{cases} \frac{4}{M_{base}^2} * i & 0 < i < M_{base}/2 \\ -\frac{4}{M_{base}^2} * i + \frac{4}{M_{base}} & M_{base}/2 < i < M_{base} \end{cases} \tag{A.22}$$

where U is a triangular hydrograph of area 1 and a base integer $MAXBAS$ (d) representing the duration of the hydrograph.

A.0.2 Routing component

Muskingum-Cunge routing model is utilized to route runoff responses generated from the HRUs through the stream network. Each stream reach k has a storage given by:

$$S_k^t = K\left[eQ_{in} + (1-e)Q_{out}\right], \tag{A.23}$$

which is a discharge-storage equation where K (d) and e (dimensionless) are parameters controlling the celerity and dispersion of the wave routed through the channel respectively.

In this model, the discharge-storage relationship is substituted with a finite-difference form of the continuity equation $\frac{S_j^{t+1}-S_j^t}{\Delta t} = Q_{in} - Q_{out}$ to facilitate a multi-reach system with lateral inflows injected to the upstream of reach dreaming $HRU\ j$ at an average constant rate through timestep t q_j^{t+1}. The result of this is:

$$Q_j^{t+1}\left[K_j(1-e_j) + 0.5\Delta t\right] + Q_{j-1}^{t+1}\left[K_j e_j - 0.5\Delta t\right] \tag{A.24}$$

$$= Q_j^t\left[K_j(1-e_j) - 0.5\Delta t\right] + Q_{j-1}^t\left[K_j e_j + 0.5\Delta t\right] \tag{A.25}$$

$$+ q_j^{t+1}\left[K_j(1-e_j) + 0.5\Delta t\right] \tag{A.26}$$

Each HRU contains one reach with both an upstream and a downstream node. Streamflow reaches $j = 1, ..., J$ are integrated with respect to time using a first-order explicit finite difference scheme. The system of J equations can be assembled as a linear system:

$$\mathbf{AQ^{t+1}} = \mathbf{B} \tag{A.27}$$

$\mathbf{Q^{t+1}}$ is a vector of unknown streamflows at time $t+1$ solved each time step for every reach in J. The vectors $\mathbf{A}$ and $\mathbf{B}$ are functions of the model states and parameters at t:

$$\mathbf{A} \equiv (\mathbf{a} + \mathbf{\Phi b})^T \tag{A.28}$$

$$\mathbf{B} \equiv (\mathbf{d} + \mathbf{\Phi c})^T \mathbf{Q}^t + \mathbf{I}(\mathbf{a} \odot \mathbf{q}^{t+1}) \tag{A.29}$$

where $\mathbf{\Phi}$ is a JxJ sparse connectivity (0,1)-matrix defining which pairs of nodes are connected. Flow direction is from row nodes to column nodes. All rows representing upstream nodes of $HRUs$ that drain an outlet node are zeros. Lastly:

$$\mathbf{a} = \mathbf{I}(\mathbf{K} - \mathbf{K} \odot \mathbf{e}) + dt * 0.5 \tag{A.30}$$

$$\mathbf{b} = \mathbf{I}(\mathbf{K} \odot \mathbf{e}) - dt * 0.5 \tag{A.31}$$

$$\mathbf{c} = \mathbf{I}(\mathbf{K} - \mathbf{K} \odot \mathbf{e}) - dt * 0.5) \tag{A.32}$$

$$\mathbf{d} = \mathbf{I}(\mathbf{K} \odot \mathbf{e}) + dt * 0.5 \tag{A.33}$$

$\mathbf{K}$ is an identity matrix of order J. e and $\mathbf{K}$ are column vectors holding parameters e and K for every reach in N. The $\odot$ operator denotes the Schur (elementwise) product between two vectors. The solution of (A.27) will become unstable if $\Delta t > 2 * K_j * (1 - e_j)$. To guard against this an an adaptive time stepping scheme was implemented. In this adaptive scheme the default timestep is reduced by an integer fraction until the stability condition is satisfied within all reaches.

Bibliography

[1] Jeffrey L. Anderson, Stephen L. Anderson, Jeffrey L. Anderson, and Stephen L. Anderson. A Monte Carlo Implementation of the Nonlinear Filtering Problem to Produce Ensemble Assimilations and Forecasts. *Monthly Weather Review*, 127(12):2741–2758, dec 1999.

[2] J. D. Annan, D. J. Lunt, J. C. Hargreaves, and P. J. Valdes. Parameter estimation in an atmospheric GCM using the Ensemble Kalman Filter. *Nonlinear Processes in Geophysics*, 12(3):363–371, feb 2005.

[3] A. Bárdossy. Calibration of hydrological model parameters for ungauged catchments. jan 2007.

[4] S. Beldring, K. Engeland, L. A. Roald, N. R. Sælthun, and A. Voksø. Estimation of parameters in a distributed precipitation-runoff model for Norway. *Hydrology and Earth System Sciences*, 2003.

[5] S. Bergström. The HBV model - its structure and applications. *Swedish Meteorological and Hydrological Institute Reports Hydrology*, 1992.

[6] Sten Bergström. Development and Application of a Conceptual Runoff Model for Scandinavian Catchments. *Smhi*, 1976.

[7] G. Blöschl and M. Sivapalan. Scale issues in hydrological modelling: A review. *Hydrological Processes*, 9(3-4):251–290, apr 1995.

[8] M. Chen, S. Liu, L.L. Tieszen, and D.Y. Hollinger. An improved state-parameter analysis of ecosystem models using data assimilation. *Ecological Modelling*, 219(3-4):317–326, dec 2008.

[9] L.W Mays V.T Chow D.R Maidment. Unit Hydrograph. In *Applied Hydrology*. McGraw-Hill, New York, 1988.

[10] Geir Evensen. Sequential data assimilation with a nonlinear quasi-geostrophic model using Monte Carlo methods to forecast error statistics. *Journal of Geophysical Research*, 99(C5):10143, may 1994.

[11] Geir Evensen and Geir Evensen. Advanced Data Assimilation for Strongly Nonlinear Dynamics. *Monthly Weather Review*, 125(6):1342–1354, jun 1997.

[12] Andrew Gelman, John B. Carlin, Hal S. Stern, David B. Dunson, Aki Vehtari, Donald B. Rubin, John B. Carlin, Hal S. Stern, David B. Dunson, Aki Vehtari, and Donald B. Rubin. *Bayesian Data Analysis, Third Edition*. Chapman and Hall/CRC, nov 2018.

[13] J. Götzinger and A. Bárdossy. Comparison of four regionalisation methods for a distributed hydrological model. *Journal of Hydrology*, 333(2-4):374–384, feb 2007.

[14] H. J. Hendricks Franssen and W. Kinzelbach. Real-time groundwater flow modeling with the Ensemble Kalman Filter: Joint estimation of states and parameters and the filter inbreeding problem. *Water Resources Research*, 44(9), sep 2008.

[15] A. J. Jakeman and G. M. Hornberger. How much complexity is warranted in a rainfallâĂŘrunoff model? *Water Resources Research*, 1993.

[16] Andrew H. Jazwinski. Stochastic Processes and Filtering. *Mathematics in Science and Enginerring*, 1970.

[17] Simon J. Julier and Jeffrey K. Uhlmann. New extension of the Kalman filter to nonlinear systems. volume 3068, page 182. International Society for Optics and Photonics, jul 1997.

[18] R. E. Kalman. A New Approach to Linear Filtering and Prediction Problems. *Journal of Basic Engineering*, 82(1):35, mar 1960.

[19] Fang Liu and Fang Liu. Bayesian Time Series: Analysis Methods Using Simulation-Based Computation. 2000.

[20] Yuqiong Liu and Hoshin V. Gupta. Uncertainty in hydrologic modeling: Toward an integrated data assimilation framework. *Water Resources Research*, 43(7), jul 2007.

[21] Marco Maneta, Susanne Schnabel, and Victor Jetten. Continuous spatially distributed simulation of surface and subsurface hydrological processes in a small semiarid catchment. *Hydrological Processes*, 22(13):2196–2214, jun 2008.

[22] Stefano Mariani and Alberto Corigliano. Impact induced composite delamination: state and parameter identification via joint and dual extended Kalman filters. *Computer Methods in Applied Mechanics and Engineering*, 194(50-52):5242–5272, dec 2005.

[23] Ralf Merz and Günter Blöschl. Regionalisation of catchment model parameters. *Journal of Hydrology*, 287(1-4):95–123, feb 2004.

[24] Robert N. Miller, Michael Ghil, and François Gauthiez. Advanced Data Assimilation in Strongly Nonlinear Dynamical Systems. *Journal of the Atmospheric Sciences*, 51(8):1037–1056, apr 1994.

[25] Rodolfo Alvarado Montero, Dirk Schwanenberg, Peter Krahe, and Peer Helmke. Unified Hydrological Flow Routing for Variational Data Assimilation and Model Predictive Control. In *Procedia Engineering*, volume 154, pages 1341–1348. Elsevier Ltd, 2016.

[26] Hamid Moradkhani, Soroosh Sorooshian, Hoshin V. Gupta, and Paul R. Houser. Dual state-parameter estimation of hydrological models using ensemble Kalman filter. *Advances in Water Resources*, 28(2):135–147, feb 2005.

[27] Jason W. Osborne. Advantages of hierarchical linear modeling. Osborne, Jason W. *Research & Evaluation*, 7(1), 2000.

[28] Mc Peel, Fhs Chiew, Andrew W. Western, and Thomas a. McMahon. Extension of Unimpaired Monthly Streamflow Data and Regionalisation of Parameter Values to Estimate Streamflow in Ungauged Catchments. *National Land and Water Resources Audit Theme 1-Water Availability Extension*, 2000.

[29] Rolf H. Reichle. Data assimilation methods in the Earth sciences. *Advances in Water Resources*, 31(11):1411–1418, nov 2008.

[30] Rolf H. Reichle, Dennis B. McLaughlin, Dara Entekhabi, Rolf H. Reichle, Dennis B. McLaughlin, and Dara Entekhabi. Hydrologic Data Assimilation with the Ensemble Kalman Filter. *Monthly Weather Review*, 130(1):103–114, jan 2002.

[31] Jan Seibert. Estimation of Parameter Uncertainty in the HBV Model. *Hydrology Research*, 28(4-5):247–262, aug 1997.

[32] Jan Seibert. Regionalisation of parameters for a conceptual rainfall-runoff model. *Agricultural and Forest Meteorology*, 98-99:279–293, dec 1999.

[33] Yuning Shi, Kenneth J. Davis, Fuqing Zhang, Christopher J. Duffy, and Xuan Yu. Parameter estimation of a physically based land surface hydrologic model using the ensemble Kalman filter: A synthetic experiment. *Water Resources Research*, 50(1):706–724, jan 2014.

[34] Soroosh Sorooshian and John A. Dracup. Stochastic parameter estimation procedures for hydrologie rainfall-runoff models: Correlated and heteroscedastic error cases. *Water Resources Research*, 16(2):430–442, apr 1980.

[35] Soroosh Sorooshian, Qingyun Duan, and Vijai Kumar Gupta. Calibration of rainfallâĂŘrunoff models: Application of global optimization to the Sacramento Soil Moisture Accounting Model. *Water Resources Research*, 29(4):1185–1194, apr 1993.

[36] Wood EF. Todini E, Szollosi-Nagy A. Adaptive stateâĂŞparameter estimation algorithm for real time hydrologic forecasting; a case study. *IISA/WMO Workshop on the Recent Developments in Real Time Forecasting/Control of Water Resources Systems*, 1976.

[37] Peter A. Troch, Claudio Paniconi, and Dennis McLaughlin. Catchment-scale hydrological modeling and data assimilation. *Advances in Water Resources*, 26(2):131–135, feb 2003.

[38] Jasper A. Vrugt, Cees G. H. Diks, Hoshin V. Gupta, Willem Bouten, and Jacobus M. Verstraten. Improved treatment of uncertainty in hydrologic modeling: Combining the strengths of global optimization and data assimilation. *Water Resources Research*, 41(1), jan 2005.

[39] Thorsten Wagener and Howard S. Wheater. Parameter estimation and regionalization for continuous rainfall-runoff models including uncertainty. *Journal of Hydrology*, 320(1-2):132–154, mar 2006.

[40] Markus Wallner, Uwe Haberlandt, and Jörg Dietrich. A one-step similarity approach for the regionalization of hydrological model parameters based on self-organizing maps. *Journal of Hydrology*, 2013.

[41] Xian-Huan Wen and Wen H. Chen. Real-Time Reservoir Model Updating Using Ensemble Kalman Filter With Confirming Option. *SPE Journal*, 11(04):431–442, dec 2006.

[42] Mike West. Mixture models, Monte Carlo, Bayesian updating, and dynamic models. *Computing Science and Statistics*, 1993.

[43] Mengsi Xiong, Pan Liu, Lei Cheng, Chao Deng, Ziling Gui, Xiaojing Zhang, and Yanghe Liu. Identifying time-varying hydrological model parameters to improve simulation efficiency by the ensemble Kalman filter: A joint assimilation of streamflow and actual evapotranspiration. *Journal of Hydrology*, 568:758–768, jan 2019.